





Measurement report: Comprehensive Seasonal Study of the

Composition and Sources of Submicron Aerosol during the

JULIAC Campaign in Germany

- Lu Liu^{1,2}, Thorsten Hohaus¹, Andreas Hofzumahaus¹, Frank Holland¹, Hendrik Fuchs^{1,3}, Ralf Tillmann¹, Birger 4
- Bohn¹, Stefanie Andres¹, Zhaofeng Tan^{1, 4}, Franz Rohrer¹, Vlassis A, Karydis¹, Vaishali Vardhan^{1, 5}, Philipp
- 6 Franke¹, Anne C. Lange¹, Anna Novelli¹, Benjamin Winter¹, Changmin Cho^{1, 6}, Iulia Gensch¹, Sergej Wedel¹,
- 7 Andreas Wahner1, and Astrid Kiendler-Scharr1,#
- 8 ¹ Institute of Climate and Energy Systems, ICE-3: Troposphere, Forschungszentrum Jülich GmbH, Jülich,
- 9 Germany
- 10 ² Center for Energy and Environmental Sciences, Paul Scherrer Institute, Villigen, Switzerland
- 11 ³ Department of Physics, University of Cologne, Cologne, Germany
- 12 ⁴ College of Environmental Sciences and Engineering, Peking University, Beijing, China
- 13 ⁵ Environmental Research Institute, University College Cork, Cork, Ireland
- 14 ⁶ Earth System Science Laboratory, National Center for Atmospheric Research (NCAR), Boulder, USA
- # deceased 15
- 16 Correspondence to: Lu Liu (lu.liu1@psi.ch), and Thorsten Hohaus (t.hohaus@fz-juelich.de)

- 18 **Abstract.** The seasonal variations of aerosol sources and their atmospheric evolution are investigated using
- 19 observations from the year-long JULIAC campaign (January-November 2019) in Jülich, Germany. Non-
- 20 refractory submicron aerosol components were continuously measured alongside oxidants (OH, O3, NO3), trace
- 21 gases, and meteorological conditions. Organic aerosols (OA) dominated the aerosol composition throughout the
- 22 year (39-58%), with secondary formation being the major source. OA, including organic nitrate and
- 23 organosulfur, peaked during a summer heatwave event due to enhanced daytime and nighttime secondary OA
- 24 formation driven by elevated concentrations of atmospheric oxidants. Changes in the OA composition during
- 25 the heatwave suggest shifts in the formation pathways, where isoprene may play an important role. Biomass-
- 26 burning, mainly wildfires and anthropogenic activities (e.g., heating, industry), is the dominant primary OA
- 27 source (45-83%), which may grow in influence due to climate change and the expected energy transition. Air
- 28 masses containing OA from regional transport from marine and wildfire sources are identified through source
- 29 apportionment. Analysis and modeling prove this method to be more reliable than traditional tracer-based
- 30 methods. Regional transport to this study site typically shows a cleansing effect on the aerosol concentration,
- 31 except in winter. Furthermore, seasonal variations in the effects of regional transport are seen, where identical
- 32 transport pathways led to different influences on aerosol properties, driven by seasonal differences in biogenic





- 33 and anthropogenic emissions. This study enhances understanding of seasonal variation in submicron aerosol
- 34 properties in response to their sources, atmospheric evolution, and transport.

1 Introduction

- 36 Atmospheric submicron aerosols affect air quality, climate-ecology interaction (Boucher et al., 2013;
- Ramanathan et al., 2001), and also human health (Dockery et al., 1993; Dockery and Stone, 2007; Pope and
- 38 Dockery, 2006; Lelieveld et al., 2015). The chemical and physical properties of aerosols change according to
- 39 diverse primary emissions, secondary formations, and their chemical transformation (e.g., oligomerization,
- 40 fragmentation, photochemical aging) in the atmosphere (Canagaratna et al., 2010; Jimenez et al., 2009; Ng et al.,
- 41 2010). Hence, their effect on the climate by direct and indirect radiative forcing varies (Fanourgakis et al., 2019;
- 42 Myhre et al., 2013). Therefore, understanding the processes determining the aerosol properties and their
- 43 corresponding emissions and secondary formation are essential for evaluating aerosol climate effects.
- 44 Among submicron aerosol compounds, organic aerosols (OA) contribute 20% to 90% of the total submicron
- 45 aerosol mass in the troposphere (Zhang et al., 2007; Jimenez et al., 2009), thus playing a key role in altering the
- 46 environmental impact of aerosols. OA can be emitted directly from primary sources, including anthropogenic
- 47 activities (e.g., residential heating, traffic exhaust) and biogenic sources (e.g., wildfire). Additionally, abundant
- 48 secondary OA (SOA) forms predominantly via atmospheric oxidation of various biogenic and anthropogenic
- 49 volatile organic compounds (VOCs) by different oxidants (OH, O₃, and NO₃). For example, the particular
- organic nitrate, as a typical secondary species mainly formed via NO₃ oxidation (Xu et al., 2015b; Lee et al.,
- 51 2016), has been shown to contribute 34% to 44% of measured submicron aerosol nitrate on a continental scale
- 52 (Kiendler-Scharr et al., 2016). Organosulfur, another important SOA component, which is essential for
- 53 determining aerosol physicochemical properties, affects the formation of cloud condensation nuclei (CCN)
- 54 (Chen et al., 2019). However, sources of organosulfur compounds in the atmosphere are diverse, originating
- from both gas-phase (Yang et al., 2023) and liquid-phase chemistry (Tan et al., 2022a). While the prevailing
- 56 view has been that interactions between anthropogenic and biogenic sources primarily contribute to the
- 57 formation of organosulfur compounds, a recent study (Bruggemann et al., 2020) suggests that reactions of
- 58 purely anthropogenic precursor species or direct emissions from fossil fuel and biomass-burning may contribute
- 59 significantly to the formation of organosulfur compounds. Nevertheless, the sources and formation mechanisms
- 60 of organosulfur compounds remain uncertain and require further studies.
- 61 To investigate the complex sources and evolution of OA, receptor models are commonly used to analyze the OA
- 62 composition, identifying several source factors. These factors primarily include primary OA (POA) components,
- as well as oxidized OA (OOA) formed through secondary oxidation, as shown in Figure 1. Previous ambient
- 64 studies aiming to identify sources primarily attributed OOA formation to photochemical processes (Hildebrandt
- et al., 2010; Jimenez et al., 2009; Sun et al., 2012; Kostenidou et al., 2015), like less oxidized oxygenated OA
- 66 (LO-OOA) and more oxidized oxygenated OA (MO-OOA) in Figure 1. However, laboratory experiments have
- demonstrated significant OOA production from nocturnal chemistry (Fry et al., 2009; Ng et al., 2008), which
- has also been supported by model simulations (Hoyle et al., 2007; Pye et al., 2010; Russell, 2005).
- 69 Observational studies further suggest night-time OOA formation, as evidenced by observations of the





enhancement of oxidized OA during the night (Saarikoski et al., 2012; Crippa et al., 2013; Florou et al., 2017; Cheng et al., 2021). The study by Liu et al. (Liu et al., 2024), which investigates data from the JULIAC campaign, highlights nocturnal OOA formation (marked as NO-OOA in Figure 1) from NO₃ oxidation during all seasons. Building upon this finding, the present study provides a more detailed analysis of the seasonal variations of nocturnal OOA formation from the perspective of its precursors.

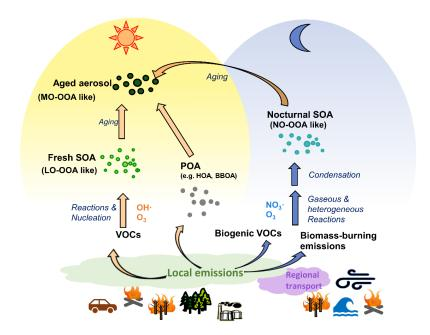


Figure 1: Overview of sources and evolution processes of organic aerosol identified in this study.

In addition to local primary emissions and secondary formation, long-term regional transport affects atmospheric conditions as well as aerosol properties. For example, methanesulfonic acid (MSA, CH₃SO₃H) is a secondary product from the oxidation of dimethyl sulfide (Zorn et al., 2008; Ge et al., 2012) and can affect CCN activity and, therefore, affect climate (Yan et al., 2019). MSA is widely regarded as a tracer for marine air transport because its precursor, dimethyl sulfide, is primarily produced by phytoplankton and anaerobic bacteria in the ocean (Charlson et al., 1987). Methanesulfonic acid-containing organic aerosol (MSA-OA) has been resolved in previous studies, not only in the coastal and oceanic environments (Schmale et al., 2013), but also at continental sites (Crippa et al., 2014).

Several studies (Hass-Mitchell et al., 2014).

Several studies (Hass-Mitchell et al., 2024; Otu-Larbi et al., 2020; Ma et al., 2019) have analysed that strong SOA formation is associated with intensive photochemistry during heatwave events with coincident elevated O₃ and biogenic VOC (mainly isoprene) concentrations. However, the detailed changes in aerosol properties and the dominant SOA formation mechanism are less frequently discussed. In this multi-seasonal study, an unusually warm summer is observed, which is reported as the third warmest summer in Germany over the past





- 91 39 years (Matzarakis et al., 2020). Notably, that abnormal heatwave lasts ten days, with ambient air
- 92 temperatures reaching 36.6°C at 50 m above ground. The continuous measurement during the heatwave
- 93 provides a valuable case study for understanding changes in SOA formation under shifts in VOC emissions due
- 94 to heat and drought stress of vegetation. In this study, comprehensive measurements and analyses are conducted
- 95 to investigate the seasonal variations in aerosol composition, with a particular focus on organic aerosol
- 96 contributions from local primary emissions, secondary formation, and long-range regional transport. Special
- attention is given to the summer period, when a significant heatwave event occurs.

98 2 Methodology

99

2.1 Campaign site and setup

- 100 The JULIAC (Jülich Atmospheric Chemistry Project) campaign, conducted from January to November 2019 at
- 101 Forschungszentrum Jülich, Germany (50.91N, 6.41E), aimed to explore annual variations of and source
- 102 contributions to oxidant concentrations (Cho et al., 2022), the composition of gas-phase species (Tan et al.,
- 103 2022b), and submicron aerosols (Liu et al., 2024). Intensive measurements were conducted during four periods
- in the different seasons: winter (JULIAC-I: 15 January 10 February), spring (JULIAC-II: 8 April 5 May),
- 105 summer (JULIAC-III: 7 August 1 September), and autumn (JULIAC-IV: 28 October 24 November). The
- site, near a mixed forest and various anthropogenic sources such as a coal-fired power plant and a sugar factory,
- 107 is influenced by both biogenic and anthropogenic emissions. During the JULIAC campaign, ambient air was
- 108 sampled from 50 m height into the SAPHIR atmospheric chamber (Simulation of Atmospheric Photochemistry
- in a Large Reaction Chamber) (Bohn and Zilken, 2005; Bohn et al., 2005) and then analyzed by instruments
- 110 connected to the chamber, minimizing the influence from local near-ground emissions, so that the air was
- 111 representative of the region. Instruments measured radicals, trace gases, OH reactivity, and submicron aerosol
- 112 components and the aerosol size distribution.

113 2.2 Instrumentations

- 114 The physical and chemical properties of ambient submicron aerosol were measured using an Aerodyne aerosol
- 115 high-resolution time-of-flight aerosol mass spectrometer (HR-ToF-AMS), a scanning mobility particle sizer
- 116 (SMPS), and a condensation particle counter (CPC). The HR-ToF-AMS provided continuous measurements of
- mass concentrations and size distributions for non-refractory chemical components of the aerosol (e.g.,
- ammonium, nitrate, sulfate, chlorine, and organics). The SMPS scanned particles in the 10-750 nm range with a
- 119 7-minute cycle, while a standalone CPC recorded total particle concentrations (diameter >5 nm). N₂O₅
- 120 concentrations were measured by custom-built cavity ring-down spectroscopy (FZJ-CRDS), which is similar to
- the instrument described in (Wagner et al., 2011), and CO, CO₂, and CH₄ were detected by a commercial cavity
- 122 ring-down instrument (Picarro). Nitrogen oxides (NO and NO₂) were detected using a chemiluminescence
- instrument with a photolytic converter (ECO PHYSICS), while O3 levels were measured with two UV
- photometers (Ansyco 41M and Thermo Scientific 49i), both of which showed good agreement (within 5%).
- Volatile organic compounds (VOCs) were monitored with a proton transfer reaction-time of flight mass
- 126 spectrometer (PTR-ToF-MS). A spectroradiometer measured spectral actinic flux densities to determine





- photolysis frequencies (Bohn and Zilken, 2005; Bohn et al., 2005). OH, HO₂, and RO₂ radicals were measured
- 128 using the FZJ laser-induced fluorescence (LIF) instrument (Cho et al., 2021), and the total OH reactivity
- 129 (k(OH)) was measured using a laser-flash photolysis LIF instrument (Fuchs et al., 2017). Additional sensors,
- 130 such as an ultrasonic anemometer (METEK, USA-1) and humidity, temperature, and pressure sensors (Driesen
- 131 + Kern) monitored ambient 3D wind data, relative humidity, temperature, and pressure at 50 m above ground
- and inside the chamber.

2.3 Calculation of particulate organic nitrate and organosulfur concentrations

- 134 The concentration of particulate organic nitrate was calculated by an approach using nitrate fragment ratios
- 135 (NO₂+/NO+) as shown in Eq. (1) based on HR-ToF-AMS measurements (Kiendler-Scharr et al., 2016; Farmer et
- 136 al., 2010; Fry et al., 2013; Xu et al., 2015a).

$$pOrgNO_{3,frac} = \frac{(1+R_{OrgNO3}) \times (R_{measured} - R_{calib})}{(1+R_{measured}) \times (R_{OroNO3} - R_{calib})}$$
(1)

- 138 R_{measured} represents the ratio of NO₂⁺ to NO⁺ ion fragments for aerosol measurements during the JULIAC
- 139 campaign. R_{calib} represents the corresponding NO₂+/NO+ fragment ratio measured from ammonium nitrate
- during biweekly calibrations of the ionization efficiency (IE) of HR-ToF-AMS during the campaign, while
- 141 R_{OrgNO3} stands for that ratio for pure organic nitrate, with a value of 0.1 suggested by (Kiendler-Scharr et al.,
- 142 2016). Based on this method, lower-limit estimations of organic nitrate concentrations having an uncertainty of
- \pm 20% (Xu et al., 2015a; Kiendler-Scharr et al., 2016) were made in this study.

$$pOrgNO_{3,conc} = pOrgNpO_{3,frac} \times NO_{3,total}$$
 (2)

- Particulate organosulfur concentrations were calculated from total sulfates measured by HR-ToF-AMS using
- the sulfate fragment pattern method (Chen et al., 2019). The organosulfur calculation method makes use of the
- 147 varying degrees of fragmentation of ammonium sulfate, MSA, and organosulfur during AMS measurements,
- resulting in differences in the distribution of fragments, including SO⁺, SO₂⁺, SO₃⁺, HSO₃⁺, and H₂SO₄⁺. This
- method used in this study assumes that the fragment of H₂SO₄⁺ is exclusively contributed by ammonium sulfate,
- while the fragment of HSO₃⁺ originates from only ammonium sulfate and MSA. Then, the mass concentrations
- 151 of total sulfate measured by the instrument ToF-AMS could be distributed to the sulfate from ammonium
- sulfate, MSA, and organosulfur, as shown below:

$$[SO_4]_{(Ammonium Sulfate)} = \frac{H_2SO_4^+}{f(H_2SO_4^+)_{Ammonium Sulfate} \cdot \Sigma HSO} \cdot [SO_4]$$
 (3)

$$[SO_4]_{(MSA)} = \frac{(HSO_3^+ - [SO_4]_{(Ammonium Sulfate)} \cdot f(HSO_3^+)_{Ammonium Sulfate)}}{f(HSO_3^+)_{MSA} \Sigma HSO} \cdot [SO_4]$$
(4)

$$[SO4]_{(Organosulfur)} = [SO4] - [SO4]_{(Ammonium Sulfate)} - [SO4]_{(MSA)}$$
(5)

- 156 Σ HSO represents the sum of molar concentrations of fragments of SO⁺, SO₂⁺, SO₃⁺, HSO₃⁺, and H₂SO₄⁺.
- 157 $f(H_2SO_4^+)_{Ammonium\ Sulfate}$ and $f(HSO_3^+)_{Ammonium\ Sulfate}$ are the molar fractions of $H_2SO_4^+$ and HSO_3^+ normalized
- 158 to ∑HSO for ammonium sulfate, which was measured during biweekly calibrations of the ionization efficiency
- of the HR-ToF-AMS instrument during the JULIAC campaign. Similarly, $f(HSO_3^+)_{MSA}$ stands for the molar





fraction of HSO₃⁺ normalized to the Σ HSO concentration for pure MSA. The value of f(HSO₃⁺)_{MSA} =0.0587 reported by (Chen et al., 2019) was used in this study, as their work showed a similar ammonium sulfate fragment distribution to ours. However, the study by (Schueneman et al., 2021) points out that this method described above is not always reliable for identifying organosulfur. Based on that, the feasibility of this sulfate fragment pattern method is further discussed in Figure 4.

2.4 PMF analysis

Positive matrix factorization (PMF) is applied to attribute the concentrations of aerosol components to various sources (Jimenez et al., 2009; Zhang et al., 2011; Sun et al., 2012; Dai et al., 2019; Crippa et al., 2014). PMF analysis decomposes the variability of a dataset X into a matrix of factor profiles F (source profiles) and a corresponding time series matrix G (source contributions) as shown in Eq. (6). Matrix E represents residuals not attributed to any source. The PMF algorithm minimizes the sum of squared residuals e_{ij} weighted by the uncertainty σ_{ij} for all input points in X, indicated by Q as shown in Eq. (7).

$$X = G \times F + E \tag{6}$$

173
$$Q = \sum_{i=1}^{m} \sum_{j=1}^{n} \left(\frac{e_{ij}}{\sigma_{ij}}\right)^{2}$$
 (7)

To understand the seasonal variations in the sources and contributions of organic aerosols, a PMF analysis was conducted on aerosol organics concentrations (mass to charge ratio, m/z 12–160) detected by HR-ToF-AMS during all four seasons of the JULIAC campaign. The SoFi Pro software (version 8.0.3.1) (Canonaco et al., 2013) was used to control the multilinear engine (ME-2) algorithm (Paatero, 1999) for aerosol source apportionment, allowing for the incorporation of prior mass spectral information to reduce rotational ambiguity (Paatero and Hopke, 2003). A signal-to-noise (S/N) threshold of 2 was applied, and down-weighting was used for S/N values below 1 to reduce errors. Factors identified in prior studies were used as references or for constraining the PMF analysis. The SoFi panel's criteria-based selection function was employed to explore similar results based on user-defined criteria, such as correlations with relevant trace gases (e.g., CO for biomass-burning sources). The optimal PMF solution was selected based on the evaluation of parameters, residuals, factor spectra, correlations with external tracers (e.g., VOCs, radicals, wind direction), and the interpretability of the factor's variation patterns. This involved assessing key parameters (e.g., Unexplained variation (UEV)) in Table S1, characteristics of source mass spectra (Tables S2–S4), and examining the agreement between resolved source factors with their diurnal patterns, related tracer, and atmospheric conditions (Fig. S1).

2.5 Trajectory model

To understand the effect of long-term regional transport on aerosol properties, 24-h and 72-h backward trajectories with a 2-hour resolution from the sampling site were computed during the four JULIAC intensive phases using the HYSPLIT model (Version 5.0.0)(Stein et al., 2015), based on GDAS meteorological data from





194 NOAA's Air Resources Laboratory (ARL). The trajectory arrival times match the detection times of instruments 195 at the JULIAC campaign. Further analyses, like cluster analysis and concentration field (CF) statistics (Seibert 196 et al., 1994; Debevec et al., 2017), were performed using the ZeFir graphical interface (version 3.7) in Igor Pro 197 (Petit et al., 2017). Additional details on ZeFir's trajectory analysis applications are available in previous studies 198 (Debevec et al., 2021). 199 Aerosol liquid water content estimation 2.6 200 The aerosol liquid water content (ALWC) was estimated using the ISORROPIA-II thermodynamic model 201 (Fountoukis and Nenes, 2007). The model predicts the aerosol phase state and composition based on observed 202 ambient relative humidity (RH), temperature (T), and aerosol concentrations of nitrate, sulfate, chloride, 203 ammonium, sodium, and potassium. ISORROPIA-II has been widely validated with in-situ datasets and has 204 demonstrated strong performance compared to other thermodynamic equilibrium models (Nowak et al., 2006; 205 Fountoukis et al., 2009). 206 Results 207 The variations of non-refractory chemical component concentrations of submicron aerosol (NF-PM1), including 208 organics, nitrate, ammonium, chlorine, and sulfate, were measured during each season of the JULIAC 209 campaign. As shown in Table 1, the highest average concentration of NF-PM1 is observed in summer (JULIAC-210 III) (to be $7.7 \pm 4.8 \,\mu\text{g/m}^3$), which is more than seven times higher than the lowest concentration recorded in 211 winter (JULIAC-I) (with $1.1 \pm 1.0 \,\mu\text{g/m}^3$). The annual average concentration of NF-PM1 is $4.0 \,\mu\text{g/m}^3$ at this 212 semi-rural site, similar to aerosol levels reported in previous studies in Europe and the United States of America 213 (Table 1). In general, organic aerosols are the major component, accounting for 39% to 58% of the total mass of 214 submicron aerosols. Aerosol sulfate (16%-26%) is the second most abundant component, followed by nitrate 215 (5%-26%). The mass fractions of aerosol nitrate and organics show distinct seasonal patterns. During summer, 216 nitrate accounts for only 5% of the total aerosol mass, a sharp decrease compared to 23%-26% in the other 217 seasons. In contrast, organic aerosols contribute a much higher fraction in summer (58%) than in the other 218 seasons (ranging from 39% to 58%), indicating a pronounced seasonal enhancement. The sulfate fraction 219 remains relatively constant (20%-26%) throughout the year. To better understand these trends in aerosol 220 composition and concentration, we conduct a detailed comparison of the properties of organic aerosols in each 221 season. Additionally, the contributions of organic nitrate and organosulfur are estimated to evaluate the seasonal 222 formation processes contributing to these aerosol species. 223 224 Table 1 Overview of the seasonal average concentrations of components of submicron aerosol measured by HR-225 ToF-AMS, together with the total number and volume of submicron aerosol measured by SMPS, and 226 atmospheric conditions (relative humidity, RH, and ambient temperature) during the four JULIAC intensive

227

phases, compared with previous field observations.

https://doi.org/10.5194/egusphere-2025-3074 Preprint. Discussion started: 18 July 2025 © Author(s) 2025. CC BY 4.0 License.





Campaign	Total aerosol (μg·m ^{·3})	Total volume (10 ⁹ nm³·cm·³)	Total number (10 ³ cm ⁻³)	Nitrate (μg·m [*]	Sulfate (µg·m [*]	Ammonium (μg·m ⁻³)	Chlorine (μg·m ^{·3})	Organics (μg·m·³)	RH (%)	Temp (°C)	Reference
JULIAC-I, Jan-Feb 2019	1.1 ± 1.0	3.1±2.8	2.5±1.5	0.3±0.4	0.2±0.2	0.1±0.2	0.02±0.02	0.4±0.3	66±18	5±4	This study
JULIAC-II, Apr-May 2019	2.6 ± 2.6	2.2± 1.6	2.8±1.3	0.6±1.3	0.5±0.4	0.4±0.5	0.02±0.02	1.1±0.9	44±21	12±6	This study
JULIAC-III, Aug-Sep 2019	7.7 ±4.8	1.6± 1.9	4.0±1.9	0.4±0.5	2.0±1.2	0.8±0.5	0.02±0.01	4.4±3.0	45±21	21±5	This study
JULIAC-IV, Nov 2019	4.2 ± 2.3	1.1±0.7	2.4±1.3	1.0±0.8	0.7±0.4	0.5±0.3	0.04±0.03	2.0±1.1	65±15	15±5	This study
Cabauw, the Netherlands, Jul 2012- Jun 2013	6.2			1.9	0.9	0.9	0.06	2.2	82	9	(Schlag et al., 2016)
<u>Hyvtiälä</u> , Finland, Mar-Apr 2005	2.0			0.3	0.3	0.2		1.2			(Raatikainen et al., 2010)
Texas, Houston, USA, Feb 2014	6.1±4.3			1.4±1.4	1.4±0.8	0.9±0.6	0.06±0.09	2.3±1.4	76±18	9±6	(Dai et al., 2019)
Texas, Houston, USA, May 2014	3.6±2.3			0.1±0.1	1.3±0.6	0.5±0.2	0.02±0.02	1.7±1.4	72±19	24±4	(Dai et al., 2019)
Oklahoma, USA, Nov 2010-Jul 2012	7.0±9.3			1.5±3.0	0.8±1.0	0.7±1.2	0.02±0.04	4.0±6.2			(Parworth et al., 2015)





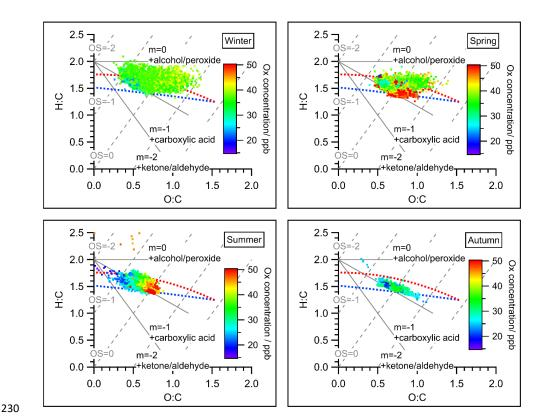


Figure 2: Van Krevelen triangle graph for all measurements of organic aerosol during the four seasons of the JULIAC campaign. Atomic ratio regions of standard groups for alcohol/peroxide, carboxylic acid, and ketone/aldehyde (Aiken et al., 2007) were marked as references. The dots in all graphs were color-coded by the concentration of the oxidant Ox (NO₂+O₃) to represent the intensity of photochemistry. The red and blue dashed line corresponds to the right and left lines of the f44/f43 triangle introduced in Ng et al. (2010, representing the lower oxidation level (like primary OA) and higher oxidation level (like secondary OA), respectively. The estimated carbon oxidation states (OSc≈2O/C-H/C) were marked as gray dashed lines. An overview of the averaged elemental ratios O:C, H:C, and OSc with corresponding standard deviations of total organic aerosol for the four JULIAC intensive phases is given in Table S5.

OA dynamically evolves in the atmosphere, converging to a higher oxidation status with time (Ng et al., 2011), which can be indicated by a high elemental O:C ratio or estimated carbon oxidation states (OSc \approx 2O/C-H/C) (Canagaratna et al., 2015). Hence, the oxidation degree of OA is a key parameter for understanding the atmospheric evolution of OA. In Figure 2, the degrees of oxidation of OA during each season are displayed in a Van Krevelen triangle (Ng et al., 2011), color-coded with O_X concentrations. O_X , defined as the sum of ozone (O₃) and nitrogen dioxide (NO₂), is a conserved quantity under photochemical cycling and is often used as a proxy for atmospheric oxidation capacity and, consequently, the intensity of secondary oxidation in the





atmosphere (Li et al., 2015; Canonaco et al., 2015). Only during summer, higher O:C ratios of OA correlate with increased O_x concentrations, suggesting the significant contribution of secondary OA formation to total OA. This assumption is further discussed and supported by the results of the source apportionment analysis presented in Section 4.1. The average oxidation degrees of OA for each season are calculated (Table S5). The overall oxidation degree of OA reaches the minimum during summer with an average O:C of 0.64 and the maximum in spring with an average O:C equal to 0.76. The difference in OA properties originates from the difference in emission sources and SOA formation mechanisms among seasons, which will be confirmed by the aerosol source apportionment analysis below (Section 4.1).

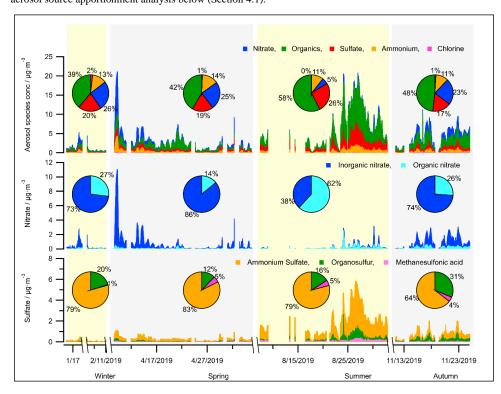


Figure 3: Seasonal variation in the concentrations of aerosol bulk components (organics, sulfate, nitrate, ammonium, chlorine) and calculated concentrations of species (organic nitrate, organosulfur, methanesulfonic acid) from HR-ToF-AMS measurements.

Particulate organic nitrates have been reported as ubiquitous components and significant contributors to organic aerosol (OA) mass in both Europe and the United States of America(Kiendler-Scharr et al., 2016; Ng et al., 2017). In this study, a high mass fraction of organic nitrate to total aerosol nitrate, up to 62%, is found during the summer (JULIAC-III) (Figure 3). This is not the first time that a high mass fraction of organic nitrate has been observed in Europe during spring or summer. For instance, the fraction of organic nitrate to total aerosol nitrate was found to be 67% at Cabauw, Netherlands in March 2008, 73% at Melpitz, Germany in March 2009, and 77% at San Pietro Capofiume, Italy, in April 2008 (Kiendler-Scharr et al., 2016). In this previous study based on combined analyses of chemistry transport models, abundant organic nitrate is found to be mainly





268 formed via the NO₃ oxidation of biogenic VOCs (especially of monoterpenes). In the JULIAC campaign, 269 significant nocturnal oxidized OA production in all seasons is observed, and rich particulate organic nitrate 270 during summer has been found to originate from the NO₃ oxidation of biogenic VOCs in a previous study (Liu 271 et al., 2024). Additionally, a high level of organic nitrate contribution, up to 20% of the submicron nitrate, is 272 observed during wintertime of the JULIAC campaign in Figure 3, which is demonstrated to be related to the 273 NO₃ chemistry of anthropogenic VOCs, such as phenolics from residential heating(Liu et al., 2024). 274 The concentration of organosulfur is the highest in summer (JULIAC-III, up to 6 µg/m³) (Figure 3), followed by 275 autumn (JULIAC-III, up to 2 µg/m³). Previous studies have reported that the most abundant aerosol 276 organosulfur species are mainly derived from the oxidation of isoprene and monoterpenes (Wang et al., 2021a). 277 The strong correlation between organosulfur compounds and biogenic OOA during summer (JULIAC-III; see 278 Fig. S2) indicates that biogenic precursors also play a dominant role in formation of organosulfur compounds 279 during this period. In addition, the high consistency between the variation of biogenic OOA and organosulfur 280 concentrations, as well as the total surface and volume of aerosols detected by SMPS (Table S6), demonstrates 281 that multi-phase reactions involving SOA and sulfur dioxide (SO₂) are one potential pathway for organosulfur 282 formation during summer. A previous chamber experiment on organosulfur formation from multiphase reactions 283 (Yao et al., 2019) emphasizes the crucial role of aerosol liquid water content (ALWC) in regulating the reactive 284 uptake coefficient of SO₂, ultimately influencing aerosol organosulfur formation. In our study, we observe 285 significantly higher organosulfur concentration during a summertime heatwave event. During the heatwave 286 event, despite a modest 10% decrease in relative humidity (RH), the ALWC increased by a factor of 2.3 287 compared to the summer period before the heatwave. This increase is likely driven by enhanced concentrations 288 of particulate sulfate, nitrate, and organics (Meng et al., 2024), which can contribute to greater aerosol 289 hygroscopicity and subsequently promote SO2 uptake and organosulfur formation. More investigations of the 290 heatwave event will be discussed in Section 4.2. Figure 3 further illustrates that the mass fraction of 291 organosulfur to the total sulfate shows a high relative value of 20-31% during cold seasons (autumn and winter) 292 compared to values of 12-16% during warmer seasons (spring and summer). Numerous laboratory studies have 293 demonstrated that organosulfur can be produced through aqueous-phase oxidation of aromatic compounds in the 294 presence of inorganic sulfate (Wang et al., 2021b; Huang et al., 2020). The elevated ALWC and enhanced 295 continuous anthropogenic activities during colder seasons, such as residential heating (Section 4.1), may further 296 promote the aqueous-phase formation of organosulfur. However, further research is required to reach a 297 definitive conclusion. 298 The feasibility of the method used here to calculate the concentration of organosulfur (Section 2.3) has been 299 previously tested using data collected in several airborne field campaigns (Schueneman et al., 2021). Results 300 show that the decomposition and fragmentation of organosulfur are affected by multiple factors, particularly in 301 environments with high aerosol acidity or elevated concentrations of ammonium nitrate. The fragmentation 302 method for the determination of organosulfur concentrations exhibits high reliability only in a narrow range of 303 aerosol acidity (pH>0) and a fraction of ammonium nitrate below 0.3. Figure 4 aims to evaluate the applicability 304 of the organosulfur method to the data derived during the JULIAC campaign. Study of (Schueneman et al., 305 2021) shows that data points located in Figure 4 condition II (ammonium nitrate fraction<0.3 and pH>0, marked 306 by red dashed box) indicate the feasibility of organosulfur fragmentation methods for the corresponding





measurement period. During the winter of this study, at a relatively low aerosol pH (<0), only 43% of the measurements fall within condition II. In contrast, during other seasons, 70% to 99% of the measurements predominantly fall within condition II.

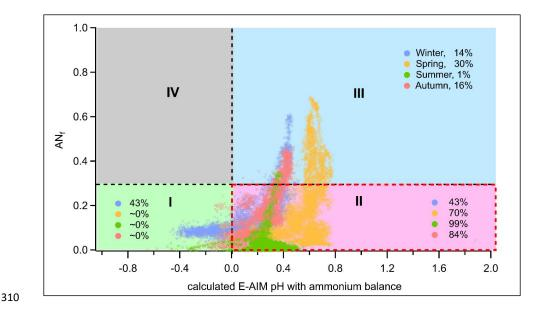


Figure 4: Distribution of aerosol data points measured during the four seasons of the JULIAC campaign for chemical conditions defined by the ammonium nitrate mass fraction (AN_f) and the pH predicted by the Extended Aerosol Inorganics Model (E-AIM) as established by (Schueneman et al., 2021). The E-AIM pH was estimated from the measured ammonium balance using HR-ToF-AMS via the empirical calculation method introduced by (Schueneman et al., 2021). For all seasons, the fractions of data points under the four conditions were calculated and displayed within the corresponding areas.

4 Discussion

4.1 Overview of seasonal sources of organic aerosols



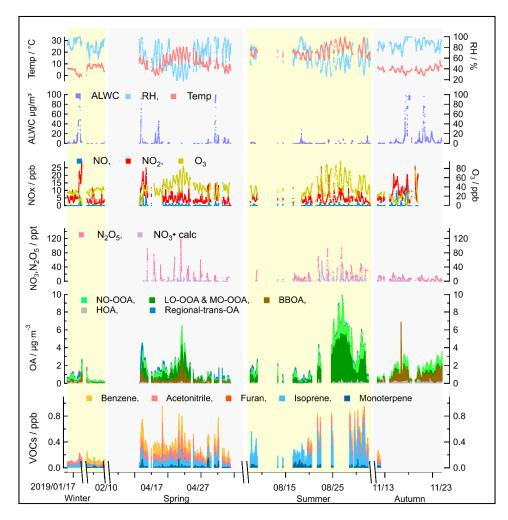


Figure 5: Overview of seasonal variations in source contributions derived from the PMF analysis of OA measurements, including supporting ambient measurements that can be used to identify sources, such as aerosol liquid water content (ALWC), trace gase concentrations (VOCs, O₃, NO₃, N₂O₅, NO₃ radicals), and meteorological parameters (temperature and RH), measured during the JULIAC campaign.

The seasonal variations of meteorological parameters (e.g., RH, wind conditions) and various tracers, including VOCs (e.g., monoterpenes, furan), radicals, trace gases (e.g., NO, NO₂, CO), are displayed in Figure 5. For the OA concentrations, the contributions of identified OA sources are illustrated. The comprehensive measurements enhance and strengthen the accuracy of the identification of primary OA sources and improve the understanding of the dominant mechanisms driving secondary OA formation (Liu et al., 2024).

Overall, secondary OA formation, consisting of low oxidized OOA (LO-OOA), more oxidized OOA (MO-OOA), and nocturnal oxidized OOA (NO-OOA), dominates the OA mass in most seasons, contributing 46% to





333

334

335

336

337

338

339

340

341

342

343

344

345

346

347

348

349

350

351

352

353

354

355 356

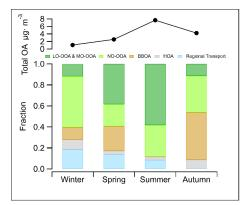
357

358

359

360

88% of total OA (Figure 5, Figure 6). The only exception was observed in autumn, when primary emissions, particularly from biomass-burning, became more abundant. Nighttime SOA formation via NO₃-initiated oxidation, represented by NO-OOA, accounts for 21% to 48% of the total OA, highlighting the importance of nocturnal oxidation processes (Liu et al., 2024). The balance of daytime (LO-OOA, MO-OOA) and nighttime (NO-OOA) oxidation varies seasonally, reflecting shifts in the dominant OA formation pathways. In summer, daytime biogenic oxidation processes dominate, contributing more than 50% of the OA mass. Conversely, during colder periods such as autumn and winter, nighttime oxidation surpasses daytime oxidation, indicating a stronger influence of nocturnal pathways. Primary and secondary OA related to biomass-burning sources comprise 83% of the total OA mass during autumn. This emphasizes the need for emission control measures targeting biomass-burning, especially with respect to residential heating and industrial activities (Section 4.1.1) to improve air quality in autumn and winter. The seasonal changes of OA source factors are displayed in the space of fCO₂⁺ (fragment fraction of CO₂⁺ in OA) vs fC₂H₃O⁺ (fragment fraction of C₂H₃O⁺ in OA) as shown in Figure 6, complemented by a correlation analysis of the source spectra (Table S2-S4). Primary emissions, represented by HOA and BBOA, cluster at low fCO2+ and low fC2H3O+ values, similar to primary source characteristics reported in previous studies (Sun et al., 2012; Zhang et al., 2015; Crippa et al., 2013; Chen et al., 2015). Seasonal variability in biomass-burning emissions is evident from the scattered distribution of BBOA (Section 4.1.1). For secondary sources, LO-OOA factors found during spring and summer have higher fC₂H₃O⁺ but lower fCO2+ than the MO-OOA factors in winter and autumn, which implies biogenic derived SOA formation during spring and summer (Canonaco et al., 2015). For nocturnal oxidation sources, NO-OOA factors cluster closely in the fCO2+ vs. fC2H3O+ space in spring, autumn and winter, while summer NO-OOA exhibits the highest fC₂H₃O⁺ and lowest fCO₂⁺ values. The distinct oxidation level of summer NO-OOA, as discussed by (Liu et al., 2024), is attributed to biogenic precursors driving NO₃-initiated oxidation in summer, in contrast to biomass-burning emissions being the precursors in the other seasons.



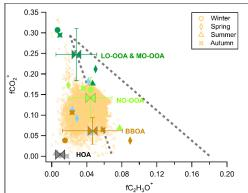


Figure 6: Left panel: Comparison of the average total mass concentration of organic aerosol measured by HR-ToF-AMS and the mass fraction of primary and secondary sources' contributions to OA during the JULIAC campaign. Right panel: fCO_2^+ (fraction of fragment CO_2^+ in OA) vs $fC_2H_3O^+$ (fraction of fragment $C_2H_3O^+$ in OA) for all organic aerosols during the JULIAC campaign (small yellow dots). The OA source factors (including LO-OOA, MO-OOA, NO-OOA, BBOA, HOA, and regional transport





factors) resolved by PMF during each season are shown in fCO₂+ vs fC₂H₃O⁺ space (the marker types representing the different seasons, the marker color stands for factor type). Mean values and standard deviations for these four types of source factors are also displayed. The coarser dashed lines represent the f44/f43 distribution triangular region of ambient OOA factors reported in (Ng et al., 2010), where f44/f43 corresponds to the mass to charge ratio of CO_2^+ (m/z 44) to $C_2H_3O^+$ (m/z 43).

4.1.1 Primary emissions of organic aerosol

The HOA factors show the lowest O:C ratios (0.03-0.13) and the highest H:C ratios (1.61-2.1) among all source factors identified in the JULIAC campaign (Fig. S3-6), consistent with previous results (DeCarlo et al., 2010; Mohr et al., 2012; Crippa et al., 2013; Sun et al., 2016). A comparison of the HOA spectra with previous studies is presented in Table S2, showing high correlation coefficients (R^2 ranging from 0.72 to 0.99) and θ , the angular distance between unit mass spectra vectors (Kostenidou et al., 2009), between 12.8° and 33.1°, which confirms the robustness of the method to identify HOA in this study. The diurnal pattern of the HOA factor shows a significant peak during the morning rush hour, indicating that traffic exhaust is the primary source. In Figure 7, the HOA factor shows the highest correlation coefficients with the traffic emission tracer gases compared to other factors, with R^2 values of 0.36 for NO, 0.35 for NO_x, 0.41 for toluene, and 0.40 for xylene. Additionally, the diurnal variations of these traffic emission tracer gases are well correlated with the variation of HOA (Fig. S7), which further supports our conclusion that the HOA source mainly represents the OA contribution from traffic emissions.

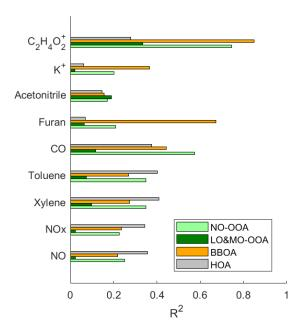


Figure 7: Cross-correlation R^2 of major organic aerosol sources among tracer gases of car exhaust (NO, NO_x, xylene, toluene), trace gases of combustion and biomass-burning (CO, furan, acetonitrile), and





382 characteristic aerosol fragments of biomass-burning (K+, C2H4O2+). OA regional transport factors are not 383 shown due to their extremely low correlation with all primary emission tracers. 384 Characteristic fragments C₂H₄O₂+ (m/z 60) and C₃H₅O₂+ (m/z 73) are well-established indicators for biomass-385 burning in AMS mass spectra (Simoneit et al., 1999; Alfarra et al., 2007). In this study, these ion mass signals 386 are prominently detected in the BBOA factor spectrum. Furthermore, the BBOA time series aligns closely with 387 the time series of fragment C₂H₄O₂+ (m/z 60) during the whole JULIAC campaign, showing the highest 388 correlation coefficient of $R^2 = 0.85$ (Figure 7). In addition, the correlation coefficients between the time series of 389 the OA factors and the biomass-burning tracers, such as furan (Akherati et al., 2020; Coggon et al., 2016) and 390 aerosol potassium (K+) (Li et al., 2003; Yu et al., 2018; Zhang et al., 2013; Tao et al., 2014) for are shown in 391 Fig. 7. The BBOA factor exhibits a significantly higher correlation value with all mentioned tracers than other 392 primary sources (HOA) and secondary sources (LO-OOA and MO-OOA), supporting its identification as 393 BBOA. The BBOA factors show a lower O:C ratio (0.28 to 0.36) than the OOA factors but a higher ratio than 394 the HOA factors, consistent with previously reported BBOA oxidation levels (Mohr et al., 2012; DeCarlo et al., 395 2010; Aiken et al., 2009). The high-resolution BBOA spectra from prior studies (Mohr et al., 2012; Hu et al., 396 2013) are similar to the BBOA spectra from each JULIAC phase (Table S3). The BBOA identified in this study 397 closely resembles findings from (Hu et al., 2013), with R² ranging from 0.76 to 0.94 and θ from 14.2° to 27.9°, 398 confirming the BBOA factor identification. 399 As mentioned above, BBOA source factors show seasonal differences (Figure 6), suggesting distinct types of 400 biomass-burning during each season. The BBOA factor observed in spring is also associated with a different 401 type of biomass-burning, as indicated by the high fC₂H₃O⁺ ratio (Fig. 6). This is confirmed to be related to the 402 regional transport of wildfire emissions (Section 4.1.3.2). The most abundant OA contribution from biomass-403 burning is found in autumn, with two distinct BBOA sources identified, which are likely related to residual 404 heating and nearby emissions from the sugar factory, which have active production of sugar only during the 405 autumn phase. Some industries in Germany, such as sugar factories, are adopting biomass fuels like beet pulp to 406 reduce fossil fuel use and achieve climate-neutral production by 2040 (Insight, 2023). This shift is part of a 407 broader energy transition that includes biomass burning as an alternative energy source (Lipiäinen et al., 2022; 408 Bataille, 2020). These changes are expected to affect anthropogenic emissions and, in turn, atmospheric 409 chemistry. 410 4.1.2 Secondary formation of organic aerosol 411 In this study, LO-OOA is predominantly observed during spring and summer, while MO-OOA is dominant 412 during autumn and winter (Fig. S3-6). Both LO-OOA and MO-OOA spectra exhibited strong contributions from 413 fragments at m/z 44 (with the signal at m/z 28 assumed to be equal to that at m/z 44 (Aiken et al., 2008)), with 414 dominant ion families C_xH_yO and $C_xH_yO_z$ (z > 1). The oxidation degrees of LO-OOA and MO-OOA are the 415 highest among OA sources in all seasons, with O:C ratios ranging from 0.7 to 1.0, comparable to previous 416 studies (Hu et al., 2013; Xu et al., 2015c; Sun et al., 2016; Dai et al., 2019). The high-resolution mass spectra of 417 LO-OOA and MO-OOA identified in this study can be compared with those of prior source apportionment studies (Mohr et al., 2012; Crippa et al., 2013; Hayes et al., 2013; Hu et al., 2013; Hu et al., 2015), with R2 0.93 418 419 - 0.99 and θ ranging from 5.9° to 15.7°. The highest similarity is observed with the results of (Hu et al., 2013).





420	LO-OOA and MO-OOA are the only source factors snowing distinct diurnal peaks around noon (Fig. 55–56), a
421	pattern characteristic of secondary organic aerosol formed through photochemical processes. High correlations
422	between O3 and LO-OOA or MO-OOA time series are observed during the warmer seasons, specifically in
423	spring and summer, with R2 values of 0.56 and 0.71, respectively. Therefore, the LO-OOA and MO-OOA
424	factors identified during the JULIAC campaign are mainly dominated by daytime oxidation processes.
425	The NO-OOA factor resolved in this study is attributed to nocturnal OOA formation dominated by NO ₃
426	chemistry, with the O:C ratios varying from 0.39 to 0.91 depending on the seasonal precursors, biogenic VOCs,
427	particularly monoterpenes in summer, and biomass-burning emissions in the colder seasons. (Liu et al., 2024).
428	The potential phase partitioning, nocturnal boundary layer development, and various reaction pathways (such as
429	ozonolysis, aqueous phase reactions, and NO_3 chemistry) have been thoroughly discussed in the study of (Liu et
430	al., 2024). That study has introduced an improved source apportionment method, using PMF analysis of aerosol
431	organic and nitrate bulk measurements to differentiate between the OOA formed from nocturnal and daytime
432	oxidation. Also, the NO-OOA factor shows typical characteristics, such as a higher ion intensity fraction of
433	$nitrate\ fragments\ (NO^+ + NO_2^+)\ normalized\ to\ the\ total\ ion\ intensity\ (f(NO^+ + NO_2^+) > 0.1)\ and\ higher\ nitrogen\ to\ nitrate\ fragments\ (NO^+ + NO_2^+) = 0.1$
434	$carbon\ ratios\ (N:C,0.05\text{-}0.15)\ than\ the\ OOA\ formed\ from\ daytime\ oxidation\ (LO-OOA\ and\ MO-OOA).\ High$
435	OA mass fractions of NO-OOA (21%-48%) highlight a significant formation via NO ₃ -initiated nocturnal
436	oxidation in all seasons.
437	Overall, secondary OA sources, represented by OOA factors (LO-OOA, MO-OOA, NO-OOA), contribute 46%-
438	88% of the total OA mass throughout the campaign. Seasonal variations in the relative contributions of daytime
439	(LO-OOA, MO-OOA) and nighttime (NO-OOA) oxidation pathways show that OOA formation is dominated
440	by daytime oxidation of biogenic VOCs in summer, while in the other seasons, nocturnal oxidation surpasses
441	daytime oxidation (MO-OOA) and predominates OOA formation.
442	4.1.3 Regional transport effect on organic aerosol
443	In this study, OA transport events are identified by a PMF analysis. These events are air masses originating from
444	marine regions or wildfires. The regional influences inferred from source factor characteristics align well with
445	trajectory model results, further supporting the PMF analysis as an appropriate method for resolving regional
446	transport events. However, the PMF analysis becomes less effective under conditions of persistent and strong
447	regional influence. For instance, during autumn, sustained strong winds can create a continuous influx of
448	regional air masses, leading to a more homogeneous aerosol composition. This continuity reduces the variability
449	needed for PMF to distinguish between distinct sources or transport patterns. Additional discussion on the
450	regional transport of OA is provided below.
451	4.1.3.1 Regional transport from the marine area
452	The OA contribution from regional transport of the marine area is attributed during spring (JULIAC-II) and
453	summer (JULIAC-III) to the MSA-OA source factor. As shown in Figure 8, the MSA-OA factor contains
454	$typical\ marker\ fragments:\ CHS^{+}(m/z\ 44.98),\ CH_{2}SO_{2}^{+}(m/z\ 77.98),\ CH_{3}SO_{2}^{+}(m/z\ 78.99),\ and\ CH_{4}SO_{3}^{+}(m/z\ 78.99),\ and\ CH_{4}SO_{3}^{+}(m$
455	95.99). Among these fragments, CH ₃ SO ₂ ⁺ is regarded to be a characteristic fragment for the MSA containing
456	ambient aerosols and has been reported as the most abundant organosulfur ion in the MSA-OA factor profile in



458

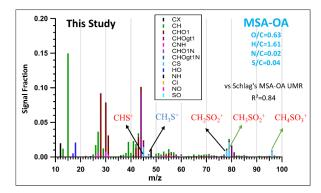
459 460

461

462



previous studies (Zorn et al., 2008; Huang et al., 2017). The MSA-OA factor in this study shows a high similarity in the marker fragments as well as in the full mass spectrum (R^2 =0.84) with the MSA-OA factor resolved by (Schlag et al., 2017). We also find the ion fragment CH_3S^+ (m/z 47.00) in the MSA-OA factor, which has been mentioned in (Schmale et al., 2013). The low intensity of the CH_3S^+ (m/z 47.00) ion mass signal may be one possible reason why it has not been reported frequently so far and is not commonly considered a stable marker ion.



463 464

465

466

467

468

479

Figure 8: MSA-OA factor profile of this study. Typical MSA marker fragments: CHS $^+$ (m/z 44.98), CH₃S $^+$ (m/z 47.00), CH₂SO₂ $^+$ (m/z 77.98), CH₃SO₂ $^+$ (m/z 78.99), and CH₄SO₃ $^+$ (m/z 95.99) are highlighted in the factor profile. Normalized ion attribution is colored by corresponding ion family groups, and elemental ratios (O/C, H/C, N/C, S/C) of the MSA-OA factor are also marked in the graph. The y-axis presents the ion signal intensity fraction.

469 In Figure 9 c), 24-hour back-trajectories (yellow) show a fast air mass transport from marine areas to the 470 measurement site, which occurred 21% of the time during spring (JULIAC-II). During this time, the 471 concentration of the MSA-OA factor increases while the contributions of other sources remain low and stable. 472 The polar diagram in Figure 9 d) shows that high MSA-OA concentrations (>0.1 µg/m³) are associated with 473 high wind speeds (>10 m/s) originating from the northwest, which align well with the marine origin trajectory. 474 Additionally, the time series of the aerosol MSA is calculated using two different characteristic ion 475 methodologies (Ge et al., 2012; Huang et al., 2015) (Figure 9 b), which also shows good agreement with the 476 variations of MSA-OA factor, with a correlation coefficient R²=0.95 for MSA-OA vs MSA (Ge method, (Ge et 477 al., 2012) and 0.94 for MSA-OA vs MSA (HKUST method, (Huang et al., 2015)). Because the MSA-OA factor 478 is not only composed of MSA but also contains other organic fragments, the concentration level of the MSA-

supports the influence of marine transport at this inland site.

OA factor is around 3 times higher than the concentration of the aerosol MSA. Overall, this comparison





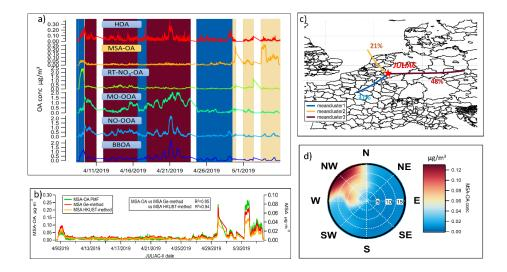


Figure 9: a) Time series of all source factors of OA resolved by the PMF analysis during spring (JULIAC-II) with the background color corresponding to different clusters of the 24-hour back-trajectories (of panel c); b) Comparison of MSA variations calculated using the Ge method (Ge et al., 2012) and the HKUST method (Huang et al., 2015), and the contribution variation of MSA-OA source resolved by PMF during spring (JULIAC-II). c) Clusters of 24-hour back-trajectories simulated by HYSPLIT4 during spring (JULIAC-II) at the Jülich site, with the proportion of each trajectory cluster marked. d) Polar diagram of MSA-OA concentration during spring, based on non-parametric wind regressions. The wind speeds are shown as the radius with the unit of m/s.

In contrast, during summer (JULIAC-III), the contribution of the MSA-OA factor and the calculated concentration of MSA (using the Ge and HKUST methods) both increase during periods when air masses are not transported from marine areas (Figure 10a). The corresponding 72-hour back trajectory cluster (Figure 10c) shows a slow movement of air masses or relatively steady conditions of the local atmosphere in summer, suggesting that local emissions are the dominant influence at the site during this period. Additionally, poor agreement of the time series in calculated MSA and MSA-OA factors is also shown, with an R² value of approximately 0.2. The strong local formation of organosulfur during summer (Figure 3) may complicate the identification of MSA and potentially introduce a bias. Another possibility is the existence of unidentified terrestrial sources for aerosol MSA formation, as suggested by previous studies (Zhou et al., 2017; Young et al., 2016; Ge et al., 2012), though the mechanisms remain unclear and warrant further investigation. However, using the mass fraction of MSA-OA normalized to the total OA and the mass fraction of MSA normalized to the total aerosol leads to notable differences in the results. In Figure 10 b, the variations in MSA-OA and MSA mass fractions show an increasing trend in their similarity (R² = 0.72–0.76) and exhibit better agreement with the back trajectory analysis. In conclusion, the observed increase in the MSA-OA concentration during the non-marine-transported period in summer could be attributed to a methodological bias or a potential unknown





formation pathway of MSA. Compared to their absolute concentration, the mass fraction of the MSA-OA factor serves as a more reliable indicator of marine transport influences, especially during summer.

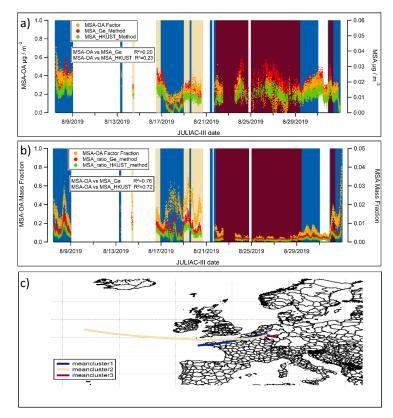


Figure 10: a) Time series of the contribution of the MSA-OA factor and the concentrations of calculated MSA using the Ge and HKUST methods during the summer (JULIAC-III), with background colors matching the corresponding back-trajectory clusters; b) Mass fraction of the MSA-OA factor (normalized to the aerosol organic mass) and MSA (normalized to the total aerosol mass) calculated using the Ge and HKUST methods during the summer (JULIAC-III); c) Clusters of 72-hour back-trajectories during the summer (JULIAC-III), simulated by HYSPLIT4.

514 4.1.3.2 Regional transport of wildfire plumes from the Russian area

A regional transport event of wildfire plumes during spring is confirmed using source apportionment analysis coupled with the analysis of 72-h back trajectories (an extension of the previous 24-h back trajectory) and the hotspot data from MODIS (Aqua & Terra) with a resolution of 1 km and VIIRS (S-NPP, NOAA-20 & NOAA-21) with a resolution of 375 m, provided by the Fire Information for Resource Management System (FIRMS) of NASA (Figure 11). Concentrated fire events are observed during spring in the Russian region and affect this study area via long-distance transport. During this time, BBOA concentrations peak in spring. This further confirms that the BBOA in spring is primarily influenced by the regional transport of fire emissions. The high frequency of fires in Russia during spring is consistent with the results of previous studies on the occurrence of





Russian wildfires (Kharuk and Ponomarev, 2017). As discussed previously (Liu et al., 2024), the nocturnal OOA formation during spring is predominantly driven by nitrate radical (NO₃) chemistry of biomass-burning emissions. Consequently, the primary organic aerosol and secondary organic aerosol (SOA) linked to the regional transport of wildfire plumes contribute to approximately half of the total organic aerosol (OA) observed during spring. This highlights wildfire emissions transport as a key factor influencing the atmospheric conditions at the site during spring.

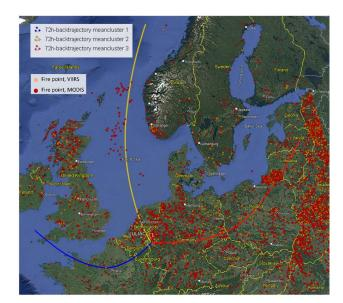


Figure 11: Trajectory clusters (yellow, blue, and red lines) of the 72-hour back-trajectories simulated by HYSPLIT4 at the measurement site in Jülich during spring (JULIAC-II). Hotspot counts during spring are shown as yellow (VIIRS) and red (MODIS) dots, provided by the Fire Information for Resource Management System (FIRMS) of NASA (accessible at https://firms.modaps.eosdis.nasa.gov/). Map background © Google Earth, image © 2025 Maxar Technologies.





4.1.3.3 Seasonal variability of regional contributions to aerosols

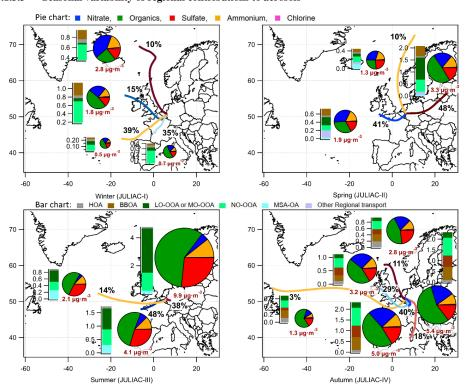


Figure 12: Trajectory clusters representing 72-hour back-trajectories simulated by HYSPLIT4 for each season at the Jülich site, annotated with the frequency proportions of each respective cluster.

Additionally, the average composition and concentration of submicron aerosols, together with the average source contributions of organics derived from PMF analysis, are presented for each corresponding cluster period.

To further understand the effect of long-range transport on the aerosol composition at the site, the back-trajectory clusters combined with the average aerosol composition and source contributions of organics during the corresponding cluster periods are analyzed. As shown in Figure 12, more than half of the long-range transport plumes originate from the west of the site. During the periods influenced by transport from these directions, the total aerosol mass consistently shows a clear decrease compared to the periods dominated by local emissions in each season, implying a general cleansing effect for the aerosol level at the site by regional transport. The only exception occurred in winter (JULIAC-I), when the aerosol mass reaches a maximum due to regional influences from air masses originating in the northwest, with an enhanced mass fraction of nitrate and an increased BBOA contribution. A clear increase in the contributions of sulfate is also observed when trajectories originate from marine regions. This increase is accompanied by a rise in the MSA-OA fraction, which is associated with the enhanced activity of phytoplankton and anaerobic bacteria in the ocean during summer, the primary natural sources of sulfur-containing compounds (Charlson et al., 1987). A similar increase in sulfate and MSA-OA is observed during spring for marine-origin transport but is absent in colder seasons.





This suggests that the seasonal activity of phytoplankton and anaerobic bacteria plays a significant role in modulating the influence of marine regional transport. In conclusion, regional influences are highly diverse, affected not only by the source regions but also by the seasonal variations in biogenic and anthropogenic activity within these regions.

4.2 Heatwave-induced changes in the formation of OOA

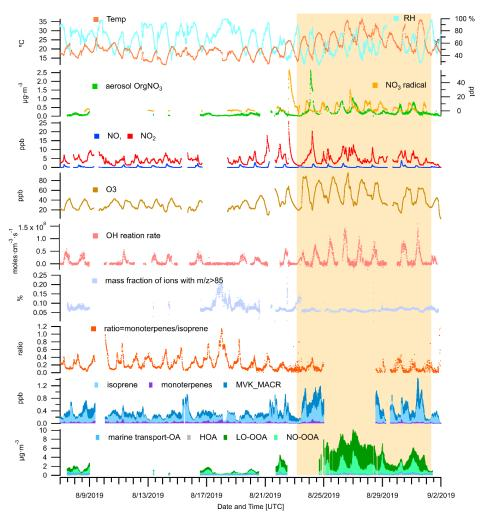


Figure 13: An overview of OA source contributions, ambient measurements of trace gases (VOCs, O₃, NO₃, N₂O₅, NO₃ radicals), meteorological parameters (temperature and RH), and calculated parameters are provided for the JULIAC summer period. The calculated parameters include the OH reaction rate





564 (derived from measured OH concentrations and OH reactivity), the mass fraction of ions with m/z > 85 in 565 OA measured by the ToF-AMS, and the concentration ratio of monoterpenes to isoprene. The period of 566 the heatwave event observed in summer is highlighted with a yellow background. 567 A previous chamber study (Mentel et al., 2013) has demonstrated that heat and drought stress can reduce 568 monoterpenes emissions, thereby suppressing biogenic OOA formation. In this study, a decrease in 569 monoterpene concentrations is observed during a heatwave event, with the average levels dropping to 60% of the pre-heatwave values(Figure 13). Conversely, isoprene concentration increases by a factor of 1.4, leading to a 570 571 substantial shift in the monoterpene-to-isoprene concentration ratio, which decreases from 0.24 to 0.11 during 572 the heatwave event. Despite the reduced monoterpene concentrations, no suppression of biogenic OOA 573 formation is observed. On the contrary, total biogenic OOA mass increases notably during the heatwave, with 574 the contribution of LO-OOA rising by a factor of 5 and NO-OOA by a factor of 3. This suggests that, beyond 575 changes in biogenic emissions, other atmospheric processes induced by the heatwave conditions play a critical 576 role in enhancing the OOA formation. 577 The increase of the atmospheric oxidation potential during heatwave events, triggered by elevated temperatures, 578 low humidity, and intense radiation, has been reported in previous studies (Desai et al., 2024; Zhang et al., 579 2024). This phenomenon is primarily reflected in the rise of the concentration of oxidants and the reaction rate 580 of BVOCs. In this study, a similar rise in atmospheric oxidation capacity is suggested by the observed increases 581 in O₃ and NO₃ concentrations, as well as the total reaction rate of OH (Cho et al., 2022), as shown in Figure 13. 582 Consequently, the enhanced formation of OOA from both daytime (LO-OOA) and nighttime (NO-OOA) 583 chemistry may be linked to this increased atmospheric oxidation potential. Additionally, the observed decrease 584 in monoterpene concentrations could be partially attributed to their faster oxidation in the presence of high 585 oxidant levels. 586 In addition, the changes in OA properties during the heatwave event are examined to assess whether shifts in the 587 dominant SOA formation pathways occurred. Figure 14 compares the average OA composition before and 588 during the heatwave, revealing a noticeable decrease in the fraction of ions with m/z > 85 relative to total ions 589 during the heatwave. This decline occurs sharply at the onset of the heatwave event, as shown in Fig. 13. 590 Additionally, although the fraction of CO2+ ions increases during the heatwave, the average O/C ratio of OA 591 remains relatively stable (0.57 before and 0.59 during the heatwave). This suggests that the shift of OA 592 composition is not driven by the increased fragmentation of highly oxygenated OA. Previous studies have used 593 the fraction of ions with m/z > 85 as an indicator for the abundance of oligomers in SOA (Faust et al., 2017; 594 Liggio and Li, 2006; Riva et al., 2019). The rapid formation of highly oxygenated organic molecules (HOM) 595 from the oxidation of BVOCs, primarily monoterpenes, is a well-known pathway for biogenic SOA formation 596 (Bianchi et al., 2019). In addition, isoprene has been reported to suppress HOM formation and subsequent SOA 597 production by OH scavenging (McFiggans et al., 2019). However, in this study, a co-increase of isoprene and 598 OOA is observed during the heatwave. As shown in Fig. 14, the isoprene-derived SOA tracer ion, CsH₆O⁺ (m/z 599 82) (Hu et al., 2015), increases in the OA during the heatwave event, with the mass fraction varying from 1.7% 600 to 4‰ (Fig. S10). When source apportionment is conducted separately for the periods before and during the 601 heatwave, the increase in C₈H₆O⁺ (m/z 82) within LO-OOA is more pronounced (Fig. S8). These findings 602 suggest a potential shift in the SOA formation pathways during the heatwave, where isoprene may play a role in





the aerosol formation and growth. Additionally, particulate organic nitrates and organosulfates both reach their annual maximum during the heatwave period (Figure 3). These findings highlight the need for further investigations of the atmospheric chemistry during heatwaves. A combination of gas- and aerosol-phase molecular measurements could provide new insights into the potential impacts of extreme heat events on SOA formation in the ambient atmosphere.

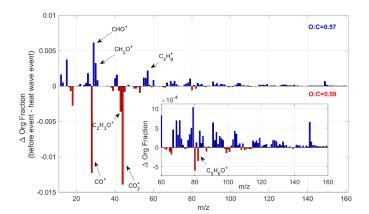


Figure 14: The change in the average organic signal mass fraction, normalized to total OA mass, between pre-heatwave and heatwave periods. The insert window shows the detailed mass spectrum difference at regions of higher molecular weight with m/z>60. The blue color bar shows the ion peaks, which have a higher intensity before the heatwave event, while the red color bar represents the ions enhanced during the heatwave event.

5 Conclusion

The 2019 Jülich Atmospheric Chemistry Project (JULIAC) campaign conducted continuous measurements of submicron aerosol composition, trace gases, and atmospheric conditions at a rural site in Germany during four seasons. Ambient air was sampled from a height of 50 m into the SAPHIR atmospheric simulation chamber, ensuring that all connected instruments sampled the same air and minimizing influence from local emissions. This study indicates that organic aerosols dominated the submicron aerosol composition throughout the year, comprising 39%-58% of the aerosol mass, followed by sulfate (16%-26%) and nitrate (5%-26%). Peak organic nitrate concentrations occur in summer, contributing up to 62% of the bulk nitrate, driven by nocturnal NO_3 oxidation. Organosulfur compounds reach their maximum concentrations in summer, likely driven by biogenic formation pathways. Interestingly, organosulfur also contributes significantly to the bulk aerosol sulfate (20%-31%) during winter and autumn, though their source remains uncertain and requires further investigation.

As the major compound of submicron aerosol, organic aerosol (OA) shows distinct seasonal variations in both mass and chemical properties. The highest OA concentrations with the lowest oxidation levels occur during summer. In contrast, autumn and winter exhibit lower OA concentrations but higher oxidation degrees, with a





629 more pronounced nocturnal increase in OA concentration. Seasonal source apportionment analysis reveals that 630 over 80% of OA mass originates from secondary OA (SOA) formed via both daytime and nighttime oxidation 631 of biogenic emissions during summer. In contrast, OA is dominated by biomass-burning sources during autumn 632 and winter, with primary OA and related SOA formation of biomass-burning sources contributing 60% to 83% 633 of OA mass. Traffic emissions are found to be a minor OA source throughout the year (3%-10%). These 634 findings suggest that effective air quality mitigation during the cold season should focus on controlling biomass-635 burning emissions, such as those from residential heating and industrial activities. In addition, the enhancement 636 of SOA formation during the heatwave is attributed to increased atmospheric oxidation potential, driven by 637 elevated oxidant levels (O₃, NO₃, and OH). A shift in SOA formation pathways during the heatwave, potentially 638 influenced by isoprene chemistry, is also observed. These findings highlight the need for further investigation 639 into heatwave-induced changes in atmospheric composition, particularly using molecular-level measurements. 640 This study examines the seasonal influence of regional transport on aerosol composition. While summer aerosol 641 composition is primarily driven by local emissions and biogenic SOA formation, regional transport significantly 642 influences the colder seasons. OA mass contributions from regional transport sources (marine, wildfire) resolved 643 by source apportionment align well with back trajectory model results, suggesting that source apportionment is a 644 more robust framework than traditional tracer-based methods for interpreting regional influences. Overall, the 645 influence of regional transport at this site generally led to a decrease in total aerosol concentration, except in 646 winter. Notably, identical regional transport pathways exhibit distinct seasonal impacts. For instance, marine 647 plumes contribute clearly to OA only in warmer seasons, driven by enhanced phytoplankton and anaerobic 648 bacterial activity. 649 Code and data availability 650 The data used in this study are available from the Jülich DATA platform (https://doi.org/10.26165/JUELICH-651 DATA/TPPXNL). 652 **Author Contributions** 653 AH designed the JULIAC campaign and coordinated its execution together with TH, HF, and FH. LL conducted 654 the aerosol measurements, performed data analysis, and drafted the manuscript. All co-authors contributed to 655 data processing and provided valuable input through extensive discussions during the manuscript preparation. 656 Competing interests 657 At least one of the (co-)authors is a member of the editorial board of Atmospheric Chemistry and Physics. 658 Acknowledgement 659 We gratefully thank all JULIAC team members for their valuable discussions and technical and logistical 660 support. We also acknowledge the use of AI-assisted tools for language polishing in preparing this manuscript.





- 662 References
- Aiken, A. C., DeCarlo, P. F., and Jimenez, J. L.: Elemental Analysis of Organic Species with Electron
- Ionization High-Resolution Mass Spectrometry, Analytical Chemistry, 79, 8350-8358,
- 665 https://doi.org/10.1021/ac071150w, 2007.
- 666 Aiken, A. C., DeCarlo, P. F., Kroll, J. H., Worsnop, D. R., Huffman, J. A., Docherty, K. S., Jimenez, J. L.: O/C
- and OM/OC Ratios of Primary, Secondary, and Ambient Organic Aerosols with High-Resolution Time-of-
- Flight Aerosol Mass Spectrometry, Environ Sci Technol, 42, 4478-4485, https://doi.org/10.1021/es703009q,
- 669 2008.
- 670 Aiken, A. C., Salcedo, D., Cubison, M. J., Huffman, J. A., DeCarlo, P. F., Ulbrich, I. M., Jimenez, J. L.: Mexico
- 671 City aerosol analysis during MILAGRO using high resolution aerosol mass spectrometry at the urban supersite
- 672 (T0) Part 1: Fine particle composition and organic source apportionment, Atmos. Chem. Phys., 9, 6633-6653,
- 673 <u>https://doi.org/10.5194/acp-9-6633-2009</u>, 2009.
- 674 Akherati, A., He, Y., Coggon, M. M., Koss, A. R., Hodshire, A. L., Sekimoto, K., Jathar, S. H.: Oxygenated
- 675 Aromatic Compounds are Important Precursors of Secondary Organic Aerosol in Biomass-Burning Emissions,
- 676 Environ Sci Technol, 54, 8568-8579, https://doi.org/10.1021/acs.est.0c01345, 2020.
- 677 Alfarra, M. R., Prevot, A. S. H., Szidat, S., Sandradewi, J., Weimer, S., Lanz, V. A., Baltensperger, U.:
- 678 Identification of the Mass Spectral Signature of Organic Aerosols from Wood Burning Emissions, Environ Sci
- 679 Technol, 41, 5770-5777, https://doi.org/10.1021/es062289b, 2007.
- 680 Bataille, C.: Low and zero emissions in the steel and cement industries: Barriers, technologies and policies,
- 681 OECD Publishing, 2020.
- 682 Bianchi, F., Kurten, T., Riva, M., Mohr, C., Rissanen, M. P., Roldin, P., Ehn, M.: Highly Oxygenated Organic
- 683 Molecules (HOM) from Gas-Phase Autoxidation Involving Peroxy Radicals: A Key Contributor to Atmospheric
- 684 Aerosol, Chem Rev, 119, 3472-3509, https://doi.org/10.1021/acs.chemrev.8b00395, 2019.
- 685 Bohn, B. and Zilken, H.: Model-aided radiometric determination of photolysis frequencies in a sunlit
- 686 atmosphere simulation chamber, Atmos. Chem. Phys., 5, 191-206, https://doi.org/10.5194/acp-5-191-2005,
- 687 2005.
- 688 Bohn, B., Rohrer, F., Brauers, T., and Wahner, A.: Actinometric measurements of NO₂ photolysis frequencies in
- the atmosphere simulation chamber SAPHIR, Atmos. Chem. Phys., 5, 493-503, https://doi.org/10.5194/acp-5-
- 690 493-2005, 2005.
- 691 Boucher, O., Randall, D., Artaxo, P., Bretherton, C., Feingold, G., Forster, P., Zhang, X. Y.: Clouds and
- aerosols, Cambridge University Press, Cambridge, UK, 2013.
- 693 Bruggemann, M., Xu, R., Tilgner, A., Kwong, K. C., Mutzel, A., Poon, H. Y., Herrmann, H.: Organosulfates in
- 694 Ambient Aerosol: State of Knowledge and Future Research Directions on Formation, Abundance, Fate, and
- Importance, Environ Sci Technol, 54, 3767-3782, https://doi.org/10.1021/acs.est.9b06751, 2020.
- 696 Canagaratna, M. R., Onasch, T. B., Wood, E. C., Herndon, S. C., Jayne, J. T., Cross, E. S., Worsnop, D. R.:
- 697 Evolution of Vehicle Exhaust Particles in the Atmosphere, Journal of the Air & Waste Management
- 698 Association, 60, 1192-1203, https://doi.org/10.3155/1047-3289.60.10.1192, 2010.
- 699 Canagaratna, M. R., Jimenez, J. L., Kroll, J. H., Chen, Q., Kessler, S. H., Massoli, P., Worsnop, D. R.: Elemental
- 700 ratio measurements of organic compounds using aerosol mass spectrometry: characterization, improved
- 701 calibration, and implications, Atmos. Chem. Phys., 15, 253-272, https://doi.org/10.5194/acp-15-253-2015, 2015.





- 702 Canonaco, F., Slowik, J. G., Baltensperger, U., and Prévôt, A. S. H.: Seasonal differences in oxygenated organic
- 703 aerosol composition: implications for emissions sources and factor analysis, Atmos Chem Phys, 15, 6993-7002,
- 704 <u>https://doi.org/10.5194/acp-15-6993-2015</u>, 2015.
- 705 Canonaco, F., Crippa, M., Slowik, J. G., Baltensperger, U., and Prévôt, A. S. H.: SoFi, an IGOR-based interface
- 706 for the efficient use of the generalized multilinear engine (ME-2) for the source apportionment: ME-2
- 707 application to aerosol mass spectrometer data, Atmos. Meas. Tech., 6, 3649-3661, https://doi.org/10.5194/amt-
- 708 6-3649-2013, 2013.
- 709 Charlson, R. J., Lovelock, J. E., Andreae, M. O., and Warren, S. G.: Oceanic phytoplankton, atmospheric
- 710 sulphur, cloud albedo and climate, Nature, 326, 655-661, https://doi.org/10.1038/326655a0, 1987.
- 711 Chen, Q., Farmer, D. K., Rizzo, L. V., Pauliquevis, T., Kuwata, M., Karl, T. G., Martin, S. T.: Submicron
- 712 particle mass concentrations and sources in the Amazonian wet season (AMAZE-08), Atmos Chem Phys, 15,
- 713 3687-3701, https://doi.org/10.5194/acp-15-3687-2015, 2015.
- 714 Chen, Y., Xu, L., Humphry, T., Hettiyadura, A. P. S., Ovadnevaite, J., Huang, S., Ng, N. L.: Response of the
- 715 Aerodyne Aerosol Mass Spectrometer to Inorganic Sulfates and Organosulfur Compounds: Applications in
- 716 Field and Laboratory Measurements, Environ Sci Technol, 53, 5176-5186,
- 717 <u>https://doi.org/10.1021/acs.est.9b00884</u>, 2019.
- 718 Cheng, Y., Ma, Y., and Hu, D.: Tracer-based source apportioning of atmospheric organic carbon and the
- 719 influence of anthropogenic emissions on secondary organic aerosol formation in Hong Kong, Atmos. Chem.
- 720 Phys., 21, 10589-10608, https://doi.org/10.5194/acp-21-10589-2021, 2021.
- 721 Cho, C., Hofzumahaus, A., Fuchs, H., Dorn, H.-P., Glowania, M., Holland, F., Novelli, A.: Characterization of a
- 722 chemical modulation reactor (CMR) for the measurement of atmospheric concentrations of hydroxyl radicals
- 723 with a laser-induced fluorescence instrument, Atmospheric Measurement Techniques, 14, 1851-1877,
- 724 https://doi.org/10.5194/amt-14-1851-2021, 2021.
- 725 Cho, C., Fuchs, H., Hofzumahaus, A., Holland, F., Bloss, W. J., Bohn, B., Novelli, A.: Experimental chemical
- 726 budgets of OH, HO2 and RO2 radicals in rural air in West-Germany during the JULIAC campaign 2019,
- 727 EGUsphere, 2022, 1-51, https://doi.org/10.5194/egusphere-2022-820, 2022.
- 728 Coggon, M. M., Veres, P. R., Yuan, B., Koss, A., Warneke, C., Gilman, J. B., de Gouw, J. A.: Emissions of
- 729 nitrogen-containing organic compounds from the burning of herbaceous and arboraceous biomass: Fuel
- 730 composition dependence and the variability of commonly used nitrile tracers, Geophysical Research Letters, 43,
- 731 9903-9912, https://doi.org/https://doi.org/10.1002/2016GL070562, 2016.
- 732 Crippa, M., DeCarlo, P. F., Slowik, J. G., Mohr, C., Heringa, M. F., Chirico, R., Baltensperger, U.: Wintertime
- 733 aerosol chemical composition and source apportionment of the organic fraction in the metropolitan area of Paris,
- 734 Atmos Chem Phys, 13, 961-981, https://doi.org/10.5194/acp-13-961-2013, 2013.
- 735 Crippa, M., Canonaco, F., Lanz, V. A., Äijälä, M., Allan, J. D., Carbone, S., Prévôt, A. S. H.: Organic aerosol
- 736 components derived from 25 AMS data sets across Europe using a consistent ME-2 based source apportionment
- 737 approach, Atmos. Chem. Phys., 14, 6159-6176, https://doi.org/10.5194/acp-14-6159-2014, 2014.
- 738 Dai, Q., Schulze, B. C., Bi, X., Bui, A. A. T., Guo, F., Wallace, H. W., Griffin, R. J.: Seasonal differences in
- 739 formation processes of oxidized organic aerosol near Houston, TX, Atmos Chem Phys, 19, 9641-9661,
- 740 <u>https://doi.org/10.5194/acp-19-9641-2019</u>, 2019.





- 741 Debevec, C., Sauvage, S., Gros, V., Salameh, T., Sciare, J., Dulac, F., and Locoge, N.: Seasonal variation and
- 742 origins of volatile organic compounds observed during 2 years at a western Mediterranean remote background
- 743 site (Ersa, Cape Corsica), Atmos. Chem. Phys., 21, 1449-1484, https://doi.org/10.5194/acp-21-1449-2021, 2021.
- 744 Debevec, C., Sauvage, S., Gros, V., Sciare, J., Pikridas, M., Stavroulas, I., Locoge, N.: Origin and variability in
- 745 volatile organic compounds observed at an Eastern Mediterranean background site (Cyprus), Atmos. Chem.
- 746 Phys., 17, 11355-11388, https://doi.org/10.5194/acp-17-11355-2017, 2017.
- 747 DeCarlo, P. F., Ulbrich, I. M., Crounse, J., de Foy, B., Dunlea, E. J., Aiken, A. C., Jimenez, J. L.: Investigation
- of the sources and processing of organic aerosol over the Central Mexican Plateau from aircraft measurements
- 749 during MILAGRO, Atmos Chem Phys, 10, 5257-5280, https://doi.org/10.5194/acp-10-5257-2010, 2010.
- 750 Desai, N. S., Moore, A. C., Mouat, A. P., Liang, Y., Xu, T., Takeuchi, M., Kaiser, J.: Impact of Heatwaves and
- 751 Declining NOx on Nocturnal Monoterpene Oxidation in the Urban Southeastern United States, Journal of
- 752 Geophysical Research: Atmospheres, 129, e2024JD041482,
- 753 https://doi.org/https://doi.org/10.1029/2024JD041482, 2024.
- 754 Dockery, D. W. and Stone, P. H.: Cardiovascular Risks from Fine Particulate Air Pollution, New England
- Journal of Medicine, 356, 511-513, https://doi.org/10.1056/NEJMe068274, 2007.
- 756 Dockery, D. W., Pope, C. A., Xu, X., Spengler, J. D., Ware, J. H., Fay, M. E., Speizer, F. E.: An Association
- 757 between Air Pollution and Mortality in Six U.S. Cities, New England Journal of Medicine, 329, 1753-1759,
- 758 https://doi.org/10.1056/NEJM199312093292401, 1993.
- 759 Fanourgakis, G. S., Kanakidou, M., Nenes, A., Bauer, S. E., Bergman, T., Carslaw, K. S., Yu, F.: Evaluation of
- 760 global simulations of aerosol particle and cloud condensation nuclei number, with implications for cloud droplet
- 761 formation, Atmos. Chem. Phys., 19, 8591-8617, https://doi.org/10.5194/acp-19-8591-2019, 2019.
- 762 Farmer, D. K., Matsunaga, A., Docherty, K. S., Surratt, J. D., Seinfeld, J. H., Ziemann, P. J., and Jimenez, J. L.:
- 763 Response of an aerosol mass spectrometer to organonitrates and organosulfates and implications for atmospheric
- 764 chemistry, Proc Natl Acad Sci U S A, 107, 6670-6675, https://doi.org/10.1073/pnas.0912340107, 2010.
- 765 Faust, J. A., Wong, J. P. S., Lee, A. K. Y., and Abbatt, J. P. D.: Role of Aerosol Liquid Water in Secondary
- 766 Organic Aerosol Formation from Volatile Organic Compounds, Environ Sci Technol, 51, 1405-1413,
- 767 <u>https://doi.org/10.1021/acs.est.6b04700</u>, 2017.
- 768 Florou, K., Papanastasiou, D. K., Pikridas, M., Kaltsonoudis, C., Louvaris, E., Gkatzelis, G. I., Pandis, S. N.:
- 769 The contribution of wood burning and other pollution sources to wintertime organic aerosol levels in two Greek
- 770 cities, Atmos Chem Phys, 17, 3145-3163, https://doi.org/10.5194/acp-17-3145-2017, 2017.
- 771 Fountoukis, C. and Nenes, A.: ISORROPIA II: a computationally efficient thermodynamic equilibrium model
- 772 for K⁺-Ca²⁺-Mg²⁺-NH₄⁺-Na⁺-SO₄²⁻-NO₃⁻-Cl⁻-H₂O aerosols, Atmos. Chem. Phys., 7, 4639-4659,
- 773 https://doi.org/10.5194/acp-7-4639-2007, 2007.
- 774 Fountoukis, C., Nenes, A., Sullivan, A., Weber, R., Van Reken, T., Fischer, M., Cohen, R. C.: Thermodynamic
- 775 characterization of Mexico City aerosol during MILAGRO 2006, Atmos. Chem. Phys., 9, 2141-2156,
- 776 <u>https://doi.org/10.5194/acp-9-2141-2009</u>, 2009.
- 777 Fry, J. L., Kiendler-Scharr, A., Rollins, A. W., Wooldridge, P. J., Brown, S. S., Fuchs, H., Cohen, R. C.: Organic
- 778 nitrate and secondary organic aerosol yield from NO_3 oxidation of β -pinene evaluated using a gas-phase
- kinetics/aerosol partitioning model, Atmos. Chem. Phys., 9, 1431-1449, https://doi.org/10.5194/acp-9-1431-1449, https://doi.org/10.5194/acp-9-1449/acp-9-
- 780 <u>2009</u>, 2009.





- 781 Fry, J. L., Draper, D. C., Zarzana, K. J., Campuzano-Jost, P., Day, D. A., Jimenez, J. L., Grossberg, N.:
- 782 Observations of gas- and aerosol-phase organic nitrates at BEACHON-RoMBAS 2011, Atmos. Chem. Phys.,
- 783 13, 8585-8605, https://doi.org/10.5194/acp-13-8585-2013, 2013.
- 784 Fuchs, H., Novelli, A., Rolletter, M., Hofzumahaus, A., Pfannerstill, E. Y., Kessel, S., Wahner, A.: Comparison
- 785 of OH reactivity measurements in the atmospheric simulation chamber SAPHIR, Atmos. Meas. Tech., 10, 4023-
- 786 4053, https://doi.org/10.5194/amt-10-4023-2017, 2017.
- 787 Ge, X. L., Zhang, Q., Sun, Y. L., Ruehl, C. R., and Setyan, A.: Effect of aqueous-phase processing on aerosol
- 788 chemistry and size distributions in Fresno, California, during wintertime, Environmental Chemistry, 9, 221-235,
- 789 https://doi.org/10.1071/en11168, 2012.
- 790 Hass-Mitchell, T., Joo, T., Rogers, M., Nault, B. A., Soong, C., Tran, M., Gentner, D. R.: Increasing
- 791 Contributions of Temperature-Dependent Oxygenated Organic Aerosol to Summertime Particulate Matter in
- 792 New York City, ACS ES&T Air, 1, 113-128, https://doi.org/10.1021/acsestair.3c00037, 2024.
- 793 Hayes, P. L., Ortega, A. M., Cubison, M. J., Froyd, K. D., Zhao, Y., Cliff, S. S., Jimenez, J. L.: Organic aerosol
- 794 composition and sources in Pasadena, California, during the 2010 CalNex campaign, Journal of Geophysical
- Research: Atmospheres, 118, 9233-9257, https://doi.org/10.1002/jgrd.50530, 2013.
- 796 Hildebrandt, L., Engelhart, G. J., Mohr, C., Kostenidou, E., Lanz, V. A., Bougiatioti, A., Pandis, S. N.: Aged
- 797 organic aerosol in the Eastern Mediterranean: the Finokalia Aerosol Measurement Experiment-2008, Atmos
- 798 Chem Phys, 10, 4167-4186, https://doi.org/10.5194/acp-10-4167-2010, 2010.
- 799 Hoyle, C. R., Berntsen, T., Myhre, G., and Isaksen, I. S. A.: Secondary organic aerosol in the global aerosol -
- 800 chemical transport model Oslo CTM2, Atmos. Chem. Phys., 7, 5675-5694, https://doi.org/10.5194/acp-7-5675-
- 801 <u>2007</u>, 2007.
- Hu, W. W., Hu, M., Yuan, B., Jimenez, J. L., Tang, Q., Peng, J. F., He, L. Y.: Insights on organic aerosol aging
- and the influence of coal combustion at a regional receptor site of central eastern China, Atmos. Chem. Phys.,
- 804 13, 10095-10112, https://doi.org/10.5194/acp-13-10095-2013, 2013.
- Hu, W. W., Campuzano-Jost, P., Palm, B. B., Day, D. A., Ortega, A. M., Hayes, P. L., Jimenez, J. L.:
- 806 Characterization of a real-time tracer for isoprene epoxydiols-derived secondary organic aerosol (IEPOX-SOA)
- from aerosol mass spectrometer measurements, Atmos Chem Phys, 15, 11807-11833,
- 808 <u>https://doi.org/10.5194/acp-15-11807-2015</u>, 2015.
- 809 Huang, D. D., Li, Y. J., Lee, B. P., and Chan, C. K.: Analysis of Organic Sulfur Compounds in Atmospheric
- 810 Aerosols at the HKUST Supersite in Hong Kong Using HR-ToF-AMS, Environ Sci Technol, 49, 3672-3679,
- 811 <u>https://doi.org/10.1021/es5056269</u>, 2015.
- 812 Huang, L., Liu, T., and Grassian, V. H.: Radical-Initiated Formation of Aromatic Organosulfates and Sulfonates
- 813 in the Aqueous Phase, Environ Sci Technol, 54, 11857-11864, https://doi.org/10.1021/acs.est.0c05644, 2020.
- Huang, S., Poulain, L., van Pinxteren, D., van Pinxteren, M., Wu, Z., Herrmann, H., and Wiedensohler, A.:
- 815 Latitudinal and Seasonal Distribution of Particulate MSA over the Atlantic using a Validated Quantification
- 816 Method with HR-ToF-AMS, Environ Sci Technol, 51, 418-426, https://doi.org/10.1021/acs.est.6b03186, 2017.
- 817 Insight, B.: German sugar manufacturer Pfeifer & Langen converts to biomass boilers, 2023.
- 818 Jimenez, J. L., Canagaratna, M. R., Donahue, N. M., Prevot, A. S., Zhang, Q., Kroll, J. H., Worsnop, D. R.:
- 819 Evolution of organic aerosols in the atmosphere, Science, 326, 1525-1529,
- 820 https://doi.org/10.1126/science.1180353, 2009.





- 821 Karanasiou, A., Alastuey, A., Amato, F., Renzi, M., Stafoggia, M., Tobias, A., Querol, X.: Short-term health
- 822 effects from outdoor exposure to biomass burning emissions: A review, Sci Total Environ, 781, 146739,
- 823 <u>https://doi.org/10.1016/j.scitotenv.2021.146739</u>, 2021.
- 824 Kharuk, V. I. and Ponomarev, E.: Spatiotemporal characteristics of wildfire frequency and relative area burned
- in larch-dominated forests of Central Siberia, Russian Journal of Ecology, 48, 507-512,
- 826 <u>https://doi.org/10.1134/S1067413617060042</u>, 2017.
- 827 Kiendler-Scharr, A., Mensah, A. A., Friese, E., Topping, D., Nemitz, E., Prevot, A. S. H., Wu, H. C.: Ubiquity of
- 828 organic nitrates from nighttime chemistry in the European submicron aerosol, Geophysical Research Letters, 43,
- 829 7735-7744, https://doi.org/10.1002/2016gl069239, 2016.
- 830 Kostenidou, E., Lee, B.-H., Engelhart, G. J., Pierce, J. R., and Pandis, S. N.: Mass Spectra Deconvolution of
- 831 Low, Medium, and High Volatility Biogenic Secondary Organic Aerosol, Environ Sci Technol, 43, 4884-4889,
- 832 <u>https://doi.org/10.1021/es803676g</u>, 2009.
- 833 Kostenidou, E., Florou, K., Kaltsonoudis, C., Tsiflikiotou, M., Vratolis, S., Eleftheriadis, K., and Pandis, S. N.:
- 834 Sources and chemical characterization of organic aerosol during the summer in the eastern Mediterranean,
- Atmos Chem Phys, 15, 11355-11371, https://doi.org/10.5194/acp-15-11355-2015, 2015.
- 836 Lee, B. H., Mohr, C., Lopez-Hilfiker, F. D., Lutz, A., Hallquist, M., Lee, L., Thornton, J. A.: Highly
- 837 functionalized organic nitrates in the southeast United States: Contribution to secondary organic aerosol and
- reactive nitrogen budgets, Proc Natl Acad Sci U S A, 113, 1516-1521,
- 839 https://doi.org/10.1073/pnas.1508108113, 2016.
- 840 Lelieveld, J., Evans, J. S., Fnais, M., Giannadaki, D., and Pozzer, A.: The contribution of outdoor air pollution
- sources to premature mortality on a global scale, Nature, 525, 367-371, https://doi.org/10.1038/nature15371,
- 842 2015
- 843 Li, J., Pósfai, M., Hobbs, P. V., and Buseck, P. R.: Individual aerosol particles from biomass burning in
- 844 southern Africa: 2, Compositions and aging of inorganic particles, Journal of Geophysical Research:
- 845 Atmospheres, 108, https://doi.org/10.1029/2002JD002310, 2003.
- 846 Li, Y. J., Lee, B. P., Su, L., Fung, J. C. H., and Chan, C. K.: Seasonal characteristics of fine particulate matter
- 847 (PM) based on high-resolution time-of-flight aerosol mass spectrometric (HR-ToF-AMS) measurements at the
- 848 HKUST Supersite in Hong Kong, Atmos Chem Phys, 15, 37-53, https://doi.org/10.5194/acp-15-37-2015, 2015.
- 849 Liggio, J. and Li, S.-M.: Reactive uptake of pinonaldehyde on acidic aerosols, Journal of Geophysical Research:
- 850 Atmospheres, 111, https://doi.org/10.1029/2005JD006978, 2006.
- 851 Lipiäinen, S., Kuparinen, K., Sermyagina, E., and Vakkilainen, E.: Pulp and paper industry in energy transition:
- 852 Towards energy-efficient and low carbon operation in Finland and Sweden, Sustainable Production and
- 853 Consumption, 29, 421-431, https://doi.org/10.1016/j.spc.2021.10.029, 2022.
- Liu, L., Hohaus, T., Franke, P., Lange, A. C., Tillmann, R., Fuchs, H., Kiendler-Scharr, A.: Observational
- 855 evidence reveals the significance of nocturnal chemistry in seasonal secondary organic aerosol formation, npj
- 856 Climate and Atmospheric Science, 7, 207, https://doi.org/10.1038/s41612-024-00747-6, 2024.
- 857 Ma, M., Gao, Y., Wang, Y., Zhang, S., Leung, L. R., Liu, C., Gao, H.: Substantial ozone enhancement over the
- 858 North China Plain from increased biogenic emissions due to heat waves and land cover in summer 2017, Atmos.
- 859 Chem. Phys., 19, 12195-12207, https://doi.org/10.5194/acp-19-12195-2019, 2019.





- 860 Matzarakis, A., Laschewski, G., and Muthers, S.: The Heat Health Warning System in Germany-Application
- and Warnings for 2005 to 2019, Atmosphere, 11, https://doi.org/10.3390/atmos11020170, 2020.
- 862 McFiggans, G., Mentel, T. F., Wildt, J., Pullinen, I., Kang, S., Kleist, E., Kiendler-Scharr, A.: Secondary organic
- aerosol reduced by mixture of atmospheric vapours, Nature, 565, 587-593, https://doi.org/10.1038/s41586-018-
- 864 0871-y, 2019.
- 865 Meng, X., Wu, Z., Chen, J., Qiu, Y., Zong, T., Song, M., Hu, M.: Particle phase state and aerosol liquid water
- 866 greatly impact secondary aerosol formation: insights into phase transition and its role in haze events, Atmos.
- 867 Chem. Phys., 24, 2399-2414, https://doi.org/10.5194/acp-24-2399-2024, 2024.
- 868 Mentel, T. F., Kleist, E., Andres, S., Dal Maso, M., Hohaus, T., Kiendler-Scharr, A., Wildt, J.: Secondary
- 869 aerosol formation from stress-induced biogenic emissions and possible climate feedbacks, Atmos. Chem. Phys.,
- 870 13, 8755-8770, https://doi.org/10.5194/acp-13-8755-2013, 2013.
- 871 Mohr, C., DeCarlo, P. F., Heringa, M. F., Chirico, R., Slowik, J. G., Richter, R., Prévôt, A. S. H.: Identification
- 872 and quantification of organic aerosol from cooking and other sources in Barcelona using aerosol mass
- 873 spectrometer data, Atmos Chem Phys, 12, 1649-1665, https://doi.org/10.5194/acp-12-1649-2012, 2012.
- 874 Myhre, G., Samset, B. H., Schulz, M., Balkanski, Y., Bauer, S., Berntsen, T. K., Zhou, C.: Radiative forcing of
- the direct aerosol effect from AeroCom Phase II simulations, Atmos. Chem. Phys., 13, 1853-1877,
- 876 <u>https://doi.org/10.5194/acp-13-1853-2013</u>, 2013.
- 877 Ng, N. L., Canagaratna, M. R., Jimenez, J. L., Chhabra, P. S., Seinfeld, J. H., and Worsnop, D. R.: Changes in
- organic aerosol composition with aging inferred from aerosol mass spectra, https://doi.org/10.5194/acpd-11-
- 879 <u>7095-2011,</u> 2011.
- 880 Ng, N. L., Kwan, A. J., Surratt, J. D., Chan, A. W. H., Chhabra, P. S., Sorooshian, A., Seinfeld, J. H.: Secondary
- 881 organic aerosol (SOA) formation from reaction of isoprene with nitrate radicals (NO₃), Atmos. Chem. Phys., 8,
- 882 4117-4140, https://doi.org/10.5194/acp-8-4117-2008, 2008.
- 883 Ng, N. L., Canagaratna, M. R., Zhang, Q., Jimenez, J. L., Tian, J., Ulbrich, I. M., Worsnop, D. R.: Organic
- 884 aerosol components observed in Northern Hemispheric datasets from Aerosol Mass Spectrometry, Atmos.
- 885 Chem. Phys., 10, 4625-4641, https://doi.org/10.5194/acp-10-4625-2010, 2010.
- 886 Ng, N. L., Brown, S. S., Archibald, A. T., Atlas, E., Cohen, R. C., Crowley, J. N., Zaveri, R. A.: Nitrate radicals
- and biogenic volatile organic compounds: oxidation, mechanisms, and organic aerosol, Atmos. Chem. Phys., 17,
- 888 2103-2162, https://doi.org/10.5194/acp-17-2103-2017, 2017.
- 889 Nowak, J. B., Huey, L. G., Russell, A. G., Tian, D., Neuman, J. A., Orsini, D., Fehsenfeld, F. C.: Analysis of
- 890 urban gas phase ammonia measurements from the 2002 Atlanta Aerosol Nucleation and Real-Time
- 891 Characterization Experiment (ANARChE), Journal of Geophysical Research: Atmospheres, 111,
- 892 https://doi.org/https://doi.org/https://doi.org/https://doi.org/10.1029/2006JD007113, 2006.
- 893 Otu-Larbi, F., Bolas, C. G., Ferracci, V., Staniaszek, Z., Jones, R. L., Malhi, Y., Ashworth, K.: Modelling the
- 894 effect of the 2018 summer heatwave and drought on isoprene emissions in a UK woodland, Glob Chang Biol,
- 895 26, 2320-2335, https://doi.org/10.1111/gcb.14963, 2020.
- 896 Paatero, P.: The Multilinear Engine: A Table-Driven, Least Squares Program for Solving Multilinear Problems,
- 897 including the n-Way Parallel Factor Analysis Model, Journal of Computational and Graphical Statistics, 8, 854-
- 898 888, https://doi.org/10.2307/1390831, 1999.





- 899 Paatero, P. and Hopke, P. K.: Discarding or downweighting high-noise variables in factor analytic models,
- 900 Analytica Chimica Acta, 490, 277-289, https://doi.org/10.1016/S0003-2670(02)01643-4, 2003.
- 901 Parworth, C., Fast, J., Mei, F., Shippert, T., Sivaraman, C., Tilp, A., Zhang, Q.: Long-term measurements of
- 902 submicrometer aerosol chemistry at the Southern Great Plains (SGP) using an Aerosol Chemical Speciation
- 903 Monitor (ACSM), Atmospheric Environment, 106, 43-55, https://doi.org/10.1016/j.atmosenv.2015.01.060,
- 904 2015.
- 905 Petit, J. E., Amodeo, T., Meleux, F., Bessagnet, B., Menut, L., Grenier, D., Favez, O.: Characterising an intense
- 906 PM pollution episode in March 2015 in France from multi-site approach and near real time data: Climatology,
- 907 variabilities, geographical origins and model evaluation, Atmospheric Environment, 155, 68-84,
- 908 <u>https://doi.org/10.1016/j.atmosenv.2017.02.012</u>, 2017.
- 909 Pope, C. A. and Dockery, D. W.: Health Effects of Fine Particulate Air Pollution: Lines that Connect, Journal of
- 910 the Air & Waste Management Association, 56, 709-742, https://doi.org/10.1080/10473289.2006.10464485,
- 911 2006
- 912 Pye, H. O. T., Chan, A. W. H., Barkley, M. P., and Seinfeld, J. H.: Global modeling of organic aerosol: the
- 913 importance of reactive nitrogen (NO_x and NO₃), Atmos Chem Phys, 10, 11261-11276,
- 914 https://doi.org/10.5194/acp-10-11261-2010, 2010.
- Raatikainen, T., Vaattovaara, P., Tiitta, P., Miettinen, P., Rautiainen, J., Ehn, M., Worsnop, D. R.:
- 916 Physicochemical properties and origin of organic groups detected in boreal forest using an aerosol mass
- 917 spectrometer, Atmos Chem Phys, 10, 2063-2077, https://doi.org/10.5194/acp-10-2063-2010, 2010.
- 918 Ramanathan, V., Crutzen, P. J., Kiehl, J. T., and Rosenfeld, D.: Aerosols, Climate, and the Hydrological Cycle,
- 919 Science, 294, 2119, https://doi.org/10.1126/science.1064034, 2001.
- 920 Riva, M., Heikkinen, L., Bell, D. M., Peräkylä, O., Zha, Q., Schallhart, S., Ehn, M.: Chemical transformations in
- 921 monoterpene-derived organic aerosol enhanced by inorganic composition, npj Climate and Atmospheric
- 922 Science, 2, https://doi.org/10.1038/s41612-018-0058-0, 2019.
- 923 Russell, M.: Predicting secondary organic aerosol formation rates in southeast Texas, Journal of Geophysical
- 924 Research, 110, https://doi.org/10.1029/2004jd004722, 2005.
- 925 Saarikoski, S., Carbone, S., Decesari, S., Giulianelli, L., Angelini, F., Canagaratna, M., Worsnop, D.: Chemical
- 926 characterization of springtime submicrometer aerosol in Po Valley, Italy, Atmos Chem Phys, 12, 8401-8421,
- 927 <u>https://doi.org/10.5194/acp-12-8401-2012</u>, 2012.
- 928 Schlag, P., Kiendler-Scharr, A., Blom, M. J., Canonaco, F., Henzing, J. S., Moerman, M., Holzinger, R.: Aerosol
- 929 source apportionment from 1-year measurements at the CESAR tower in Cabauw, the Netherlands, Atmos
- 930 Chem Phys, 16, 8831-8847, https://doi.org/10.5194/acp-16-8831-2016, 2016.
- 931 Schlag, P., Rubach, F., Mentel, T. F., Reimer, D., Canonaco, F., Henzing, J. S., Kiendler-Scharr, A.: Ambient
- and laboratory observations of organic ammonium salts in PM1, Faraday Discuss, 200, 331-351,
- 933 <u>https://doi.org/10.1039/c7fd00027h</u>, 2017.
- 934 Schmale, J., Schneider, J., Nemitz, E., Tang, Y. S., Dragosits, U., Blackall, T. D., Braban, C. F.: Sub-Antarctic
- marine aerosol: dominant contributions from biogenic sources, Atmos Chem Phys, 13, 8669-8694,
- 936 <u>https://doi.org/10.5194/acp-13-8669-2013</u>, 2013.





- 937 Schueneman, M. K., Nault, B. A., Campuzano-Jost, P., Jo, D. S., Day, D. A., Schroder, J. C., Jimenez, J. L.:
- 938 Aerosol pH indicator and organosulfate detectability from aerosol mass spectrometry measurements,
- 939 Atmospheric Measurement Techniques, 14, 2237-2260, https://doi.org/10.5194/amt-14-2237-2021, 2021.
- 940 Seibert, P., Kromp-Kolb, H., Baltensperger, U., Jost, D. T., and Schwikowski, M.: Air Pollution Modeling and
- 941 Its Application X, 1994.
- 942 Simoneit, B. R. T., Schauer, J. J., Nolte, C. G., Oros, D. R., Elias, V. O., Fraser, M. P., Cass, G. R.:
- 943 Levoglucosan, a tracer for cellulose in biomass burning and atmospheric particles, Atmospheric Environment,
- 944 33, 173-182, https://doi.org/10.1016/S1352-2310(98)00145-9, 1999.
- 945 Stein, A. F., Draxler, R. R., Rolph, G. D., Stunder, B. J., Cohen, M. D., and Ngan, F.: NOAA's HYSPLIT
- 946 atmospheric transport and dispersion modeling system, Bulletin of the American Meteorological Society, 96,
- 947 2059-2077, https://doi.org/10.1175/BAMS-D-14-00110.1, 2015.
- 948 Sun, Y., Du, W., Fu, P., Wang, Q., Li, J., Ge, X., Wang, Z.: Primary and secondary aerosols in Beijing in winter:
- 949 sources, variations and processes, Atmos Chem Phys, 16, 8309-8329, https://doi.org/10.5194/acp-16-8309-
- 950 <u>2016</u>, 2016.
- 951 Sun, Y. L., Zhang, Q., Schwab, J. J., Yang, T., Ng, N. L., and Demerjian, K. L.: Factor analysis of combined
- 952 organic and inorganic aerosol mass spectra from high resolution aerosol mass spectrometer measurements,
- 953 Atmos Chem Phys, 12, 8537-8551, https://doi.org/10.5194/acp-12-8537-2012, 2012.
- Tan, S., Zhang, X., Lian, Y., Chen, X., Yin, S., Du, L., and Ge, M.: OH Group Orientation Leads to
- 955 Organosulfate Formation at the Liquid Aerosol Surface, Journal of the American Chemical Society, 144, 16953-
- 956 16964, https://doi.org/10.1021/jacs.2c05807, 2022a.
- 957 Tan, Z., Fuchs, H., Hofzumahaus, A., Bloss, W. J., Bohn, B., Cho, C., Sommariva, R.: Seasonal variation in
- 958 nitryl chloride and its relation to gas-phase precursors during the JULIAC campaign in Germany, Atmos. Chem.
- 959 Phys., 22, 13137-13152, https://doi.org/10.5194/acp-22-13137-2022, 2022b.
- 960 Tao, J., Gao, J., Zhang, L., Zhang, R., Che, H., Zhang, Z., Hsu, S. C.: PM_{2.5} pollution in a megacity of southwest
- 961 China: source apportionment and implication, Atmos. Chem. Phys., 14, 8679-8699, https://doi.org/10.5194/acp-
- 962 14-8679-2014, 2014.
- 963 Wagner, N. L., Dubé, W. P., Washenfelder, R. A., Young, C. J., Pollack, I. B., Ryerson, T. B., and Brown, S. S.:
- 964 Diode laser-based cavity ring-down instrument for NO₃, N₂O₅, NO, NO₂ and O₃ from aircraft, Atmos. Meas.
- 965 Tech., 4, 1227-1240, https://doi.org/10.5194/amt-4-1227-2011, 2011.
- 966 Wang, Y., Zhao, Y., Wang, Y., Yu, J.-Z., Shao, J., Liu, P., Xiao, H.: Organosulfates in atmospheric aerosols in
- 967 Shanghai, China: seasonal and interannual variability, origin, and formation mechanisms, Atmos Chem Phys,
- 968 21, 2959-2980, https://doi.org/10.5194/acp-21-2959-2021, 2021a.
- 969 Wang, Y., Zhao, Y., Wang, Y., Yu, J. Z., Shao, J., Liu, P., Xiao, H.: Organosulfates in atmospheric aerosols in
- 970 Shanghai, China: seasonal and interannual variability, origin, and formation mechanisms, Atmos. Chem. Phys.,
- 971 21, 2959-2980, https://doi.org/10.5194/acp-21-2959-2021, 2021b.
- 972 Xu, L., Suresh, S., Guo, H., Weber, R. J., and Ng, N. L.: Aerosol characterization over the southeastern United
- 973 States using high-resolution aerosol mass spectrometry: spatial and seasonal variation of aerosol composition
- 974 and sources with a focus on organic nitrates, Atmos. Chem. Phys., 15, 7307-7336, https://doi.org/10.5194/acp-
- 975 <u>15-7307-2015</u>, 2015a.





- 976 Xu, L., Guo, H., Boyd, C. M., Klein, M., Bougiatioti, A., Cerully, K. M., Ng, N. L.: Effects of anthropogenic
- 977 emissions on aerosol formation from isoprene and monoterpenes in the southeastern United States, Proc Natl
- 978 Acad Sci U S A, 112, E4506-4507, https://doi.org/10.1073/pnas.1512277112, 2015b.
- 979 Xu, L., Guo, H., Boyd, C. M., Klein, M., Bougiatioti, A., Cerully, K. M., Ng, N. L.: Effects of anthropogenic
- 980 emissions on aerosol formation from isoprene and monoterpenes in the southeastern United States, Proc Natl
- 981 Acad Sci U S A, 112, 37-42, https://doi.org/10.1073/pnas.1417609112, 2015c.
- 982 Yan, J. P., Jung, J. Y., Zhang, M. M., Xu, S. Q., Lin, Q., Zhao, S. H., and Chen, L. Q.: Significant
- 983 Underestimation of Gaseous Methanesulfonic Acid (MSA) over Southern Ocean, Environ Sci Technol, 53,
- 984 13064-13070, https://doi.org/10.1021/acs.est.9b05362, 2019.
- 985 Yang, J.-R., Liu, A., and Long, B.: An unexpected feasible route for the formation of organosulfates by the gas
- 986 phase reaction of sulfuric acid with acetaldehyde catalyzed by dimethylamine in the atmosphere, Environmental
- 987 Science: Atmospheres, 3, 672-682, https://doi.org/10.1039/D2EA00159D, 2023.
- 988 Yao, M., Zhao, Y., Hu, M., Huang, D., Wang, Y., Yu, J. Z., and Yan, N.: Multiphase Reactions between
- 989 Secondary Organic Aerosol and Sulfur Dioxide: Kinetics and Contributions to Sulfate Formation and Aerosol
- 990 Aging, Environmental Science & Technology Letters, 6, 768-774, https://doi.org/10.1021/acs.estlett.9b00657,
- 991 2019.
- 992 Young, D. E., Kim, H., Parworth, C., Zhou, S., Zhang, X., Cappa, C. D., Zhang, Q.: Influences of emission
- 993 sources and meteorology on aerosol chemistry in a polluted urban environment: results from DISCOVER-AQ
- 994 California, Atmos. Chem. Phys., 16, 5427-5451, https://doi.org/10.5194/acp-16-5427-2016, 2016.
- 995 Yu, J., Yan, C., Liu, Y., Li, X., Zhou, T., and Zheng, M.: Potassium: A Tracer for Biomass Burning in Beijing?,
- 996 Aerosol and Air Quality Research, 18, 2447-2459, https://doi.org/10.4209/aaqr.2017.11.0536, 2018.
- 997 Zhang, G., Yu, X., Yin, H., Feng, C., Ma, C., Sun, S., Liu, X.: Heatwave-amplified atmospheric oxidation in a
- 998 multi-province border area in Xuzhou, China, Frontiers in Environmental Science, 12, 1496584,
- 999 https://doi.org/10.3389/fenvs.2024.1496584, 2024.
- 2000 Zhang, Q., Jimenez, J. L., Canagaratna, M. R., Ulbrich, I. M., Ng, N. L., Worsnop, D. R., and Sun, Y.:
- 1001 Understanding atmospheric organic aerosols via factor analysis of aerosol mass spectrometry: a review, Anal
- 1002 Bioanal Chem, 401, 3045-3067, https://doi.org/10.1007/s00216-011-5355-y, 2011.
- 1003 Zhang, Q., Jimenez, J. L., Canagaratna, M. R., Allan, J. D., Coe, H., Ulbrich, I., Worsnop, D. R.: Ubiquity and
- dominance of oxygenated species in organic aerosols in anthropogenically-influenced Northern Hemisphere
- midlatitudes, Geophysical Research Letters, 34, https://doi.org/https://doi.org/10.1029/2007GL029979, 2007.
- 1006 Zhang, R., Jing, J., Tao, J., Hsu, S. C., Wang, G., Cao, J., Shen, Z.: Chemical characterization and source
- apportionment of PM_{2.5} in Beijing: seasonal perspective, Atmos. Chem. Phys., 13, 7053-7074,
- 1008 https://doi.org/10.5194/acp-13-7053-2013, 2013.
- Zhang, Y. J., Tang, L. L., Wang, Z., Yu, H. X., Sun, Y. L., Liu, D., Zhou, H. C.: Insights into characteristics,
- 1010 sources, and evolution of submicron aerosols during harvest seasons in the Yangtze River delta region, China,
- 1011 Atmos Chem Phys, 15, 1331-1349, https://doi.org/10.5194/acp-15-1331-2015, 2015.
- 1012 Zhou, S., Collier, S., Jaffe, D. A., Briggs, N. L., Hee, J., Sedlacek Iii, A. J., Zhang, Q.: Regional influence of
- 1013 wildfires on aerosol chemistry in the western US and insights into atmospheric aging of biomass burning
- 1014 organic aerosol, Atmos Chem Phys, 17, 2477-2493, https://doi.org/10.5194/acp-17-2477-2017, 2017.

https://doi.org/10.5194/egusphere-2025-3074 Preprint. Discussion started: 18 July 2025 © Author(s) 2025. CC BY 4.0 License.





1015	Zorn, S. R., Drewnick, F., Schott, M., Hoffmann, T., and Borrmann, S.: Characterization of the South Atlantic
1016	marine boundary layer aerosol using an aerodyne aerosol mass spectrometer, Atmos Chem Phys, 8, 4711-4728,
1017	https://doi.org/10.5194/acp-8-4711-2008, 2008.
1018	